Journal of Solid State Electrochemistry
https://doi.org/10.1007/s10008-024-05984-6

REVIEW PAPER

Focused review on factors affecting martensitic stainless steels and super martensitic stainless steel passive film in the oil and gas field

Shoaib Malik[1] · Ahmed Bahgat Radwan[2] · Noora Al-Qahtani[2] · Aboubakr Abdullah[2] · Muhsen El Haddad[4] · Raymundo Case[3] · Homero Castaneda[3] · Noora Al-Thani[1] · Jolly Bhadra[1]

Received: 21 January 2024 / Revised: 17 June 2024 / Accepted: 18 June 2024

Abstract

Martensitic and super martensitic stainless steels are widely used in the oil and gas industry for general corrosion mitigation in the presence of sweet corrosion (CO_2) and sour corrosion (H_2S), providing a cost-effective alternative to more expensive exotic corrosion-resistant alloys. Martensitic stainless steel is an approved material for construction when selecting tubular CO_2 injection wells. This work aims to review the published literature on the subject of the operation limits of martensitic stainless steel and super martensitic stainless steel in high temperatures and high pressure under corrosive environments. Stress corrosion cracking (SCC) and sulfide stress corrosion cracking (SSCC) mechanisms on martensitic and super martensitic stainless steel surfaces are thoroughly analyzed. In this review paper, we have analyzed the factors that play a crucial role in passive film growth and passivity breakdown. The present work is to review the state of the art of mechanism responsible for SCC and SSCC susceptibility in different modified martensitic stainless steel materials, which are applied to the industry and lab scale. We have reviewed the effect of different concentrations of molybdenum content on SCC and SSCC susceptibility of conventional martensitic stainless steel, modified martensitic stainless steel, and super martensitic stainless steel. The effect of tempering temperature on the SCC and SSCC performance of the martensitic and super martensitic stainless steel was also studied. We also studied the effect of different concentrations of chromium on the improved corrosion-resistant properties and stability of passivation film.

Introduction

The development and exploitation of oil and gas reserves are complicated by the pervasive problem of corrosion. In particular, the conditions for extracting oil and gas are growing more complicated and harsher for metal pipes, resulting in their significant deterioration. This is due to the deep exploitation, the age of oil fields, and the souring of aged oil and gas reservoirs. The total direct cost of corrosion is estimated at $276 billion per year, which is 3.1% of the 1998 US gross domestic profit. Since the demand for fuel has steadily increased and fuel exploitation processes have advanced, producing from deeper and more corrosive wells has become economically feasible. These wells produce fluids with high chloride concentrations, CO_2 and H_2S environments, high pressure, and high-temperature wells, where the bottom hole pressure for high-pressure and temperature wells could exceed 1000 bar (15,000 psi) and the temperature exceeds 177 °C (350 °F) [1]. Carbon steels and low-alloyed steels have traditionally been used for downhole tubes in mildly corrosive environments. In demanding service conditions, carbon steel can experience very high corrosion rates as well as other forms of damage such as pitting [2–4] and under-deposit corrosion. Numerous anti-corrosion methods have been developed to date, and they are crucial for mitigating and preventing corrosion in oil fields. The main anti-corrosion measures currently include the use of corrosion-resistant alloys, coatings, and corrosion inhibitors, as well as their combinations [5–7]. However, using an inhibitor to prevent corrosion raises operational costs, particularly in downhole applications, where smart

✉ Jolly Bhadra
jollybhadra@qu.edu.qa

1 Qatar University Young Scientist Center, Qatar University, Doha, Qatar

2 Center for Advanced Materials, Qatar University, Doha, Qatar

3 Texas A&M University, 1111 Rellis Pkwy, Bryan, TX 77840, USA

4 Qatargas Operating Company Limited, Doha, Qatar

Published online: 09 July 2024

completion design is required for the provision of a corrosion inhibition facility. Therefore, inhibitors are used less frequently, especially given the recent emphasis on life cycle cost. The internal lining of well tubing may raise the concern of localized pitting due to detachment and delamination of lining material during well intervention operations. Stainless steels are widely used in industry due to their excellent corrosion resistance and high strength. Stainless steels are iron and chromium alloys with additional alloying elements added to change their structure and physical characteristics. They are often based on Fe–Cr, Fe–Cr-C, or Fe–Cr-Ni; at least 11% chromium is included as the primary alloying component. The corrosion protection mechanism of stainless steel is different from that of carbon steel protection and depends heavily on the integrity of the oxide film that acts as a barrier and separates stainless steel from the adjacent corrosive environment. The selection of materials for specific oil extraction processes and production units is crucial for ensuring optimal performance and longevity. The degree of protection of this oxide film depends on its adhesion, coherence, continuity, supply, and diffusivity of oxygen, and metals in the film [8] begin to deteriorate mechanically or chemically. For instance, a chloride-rich environment stimulates pitting corrosion and stress corrosion cracking (SCC) of stainless steel, which may occur under specific conditions by breaking the passive film.

In the presence of oxygen, this chromium oxide layer forms spontaneously. However, depending on the environmental parameters, it may reduce its stability, and it may more than 150 grades of stainless steel have been developed in the 100 years since the material was discovered. Special stainless steel grades with improved corrosion resistance at a wide range of temperatures were used to satisfy various industry needs. These materials typically contain high levels of Ni and Mo influence and decrease corrosion rates, as well as high levels of Cr, Mo, and Ni for passive film formation. They are divided into five distinct groups according to their crystalline structure: precipitation-hardening stainless steels, austenitic stainless steels, martensitic stainless steels, and ferritic stainless steels. Each material's service conditions and mechanical properties must be tested in conditions very similar to operational ones to determine their selection. The availability of such materials for fabrication and use in the offshore environment also influences their selection. Sulfide stress corrosion cracking (SSCC) is a significant issue, especially in sour conditions with hydrogen sulfide (H_2S). This type of corrosion affects martensitic stainless steel (MSS) and super martensitic stainless steel (SMSS) in different ways, depending on alloy composition, heat treatment, and microstructure. Understanding the mechanisms of SSCC, such as hydrogen embrittlement and the development of sulfide precipitates, provides crucial insights into how MSS and SMSS operate under harsh environments. Stress corrosion cracking (SCC) poses another significant challenge in the oil and gas industry, especially under the extreme conditions of deep wells. Both MSS and SMSS, despite their robustness and corrosion resistance, are susceptible to SCC. This vulnerability is driven by factors like temperature, pressure, chemical exposure, and specific microstructural sensitivities that can initiate cracks.

This review thoroughly analyzes factors crucial in passive film growth and passivity breakdown mechanisms on MSS and SMSS steel surfaces. The current study aims to assess the current state of the art of the mechanisms responsible for SCC and SSCC susceptibility in various modified MSS materials used in industry and research. We have reviewed the effect of different concentrations of molybdenum content on SCC and SSCC susceptibility of conventional MSS, modified MSS, and super MSS steel. We have also reviewed the different concentrations of chromium on the improved corrosion-resistant properties and stability of the MSS and SMSS passivation film under high temperature and high pressure in a corrosive environment.

Martensitic stainless steels

MSS is widely applied in the oil and gas industry for manufacturing several components, including downhole tubular, packers, wellhead, and tree components, primarily due to their durability and resistance to corrosion. Martensitic steel is an alloy family that comprises chromium, iron, and carbon as elements [9]. MSS typically contain a composition ranging from 12 to 17 wt% chromium, 0 to 4 wt% nickel, and 0.1 to 1.0 wt% carbon. Characteristics are enhanced by including additional alloying elements such as Mo, V, Nb, Al, and Cu. In hardened conditions, this stainless steel forms a martensitic crystal structure. They are ferromagnetic in nature, and when compared to other stainless steels, they have high corrosion resistance [10]. MSS are typically utilized for a variety of applications because, unlike other stainless steels, they may have their characteristics modified through heat treatment [10]. The heat treatment on MSS typically involves three different steps: the first step is austenitizing, where the steel is heated in a temperature range of 980–1050 °C, depending on steel grades. The next step is quenching; here, the austenite is transformed into martensite by using still air, pressure vacuum, or interrupted oil quenching. This is a very hard material and is too brittle for most applications. It is then followed by tempering. Here, the material is retained at a temperature of 500 °C and air-cooled. The impact resistance and elongation are increased when the tempering temperature increases and decreases the ultimate tensile strength and yield strength.

In the oil and gas industry, MSS are employed in applications that require corrosion resistance in both sweet (CO_2 corrosion) and sour (H_2S corrosion) environments. MSS can be classified into two groups based on their chemical

composition, conventional MSS, modified MSS, and super MSS. In the conventional MSS also called 13% Cr MSS with 0.22% C, 11.5–14% Cr, and up to 0.5% Ni, Ni has been used in downhole tubular applications frequently referred to as L-80 type 13Cr and 25Cr. The 13% Cr MSS is commonly applied in CO_2 environments at temperatures up to 125 °C and was introduced primarily to provide greater resistance to CO_2 corrosion over unalloyed or low-alloyed carbon steel. The modified MSS was developed in the 1990s, to improve high-temperature corrosion resistance in CO_2 environments, as well as strength from the typical 13Cr grade's 80–85 ksi range to a maximum of 110 ksi. Nickel (2–6%) and molybdenum (0.2–1.2%) additions to these modified MSS improve corrosion resistance.

Super martensitic stainless steel

The development of SMSS in the 1990s was primarily done to improve the material's resistance to high-temperature pitting corrosion in CO_2 environments with high chloride concentrations. SMSS has substantial advantages over standard martensitic–ferritic stainless steels. They contain 12–14% Cr, 4–6% Ni, 0.5–2% Mo, and < 0.03% C, along with other elements like titanium and niobium. These steels have residual austenite in the low-carbon martensite matrix structure without δ-ferrite, improving toughness and corrosion resistance [11]. They offer higher corrosion resistance, particularly in chloride conditions, as well as increased mechanical properties like toughness, strength, and impact resistance. SMSS is employed in the oil and gas industry for its mechanical properties, weldability, and corrosion resistance in chloride, CO_2, and H_2S environments [12, 13]. SMSS has been widely used for sweet and moderately sour service applications. Changes in chemical composition and microstructural structure can improve the corrosion and mechanical properties of SMSS. It is demonstrated that altering the composition of AISI 410 type stainless steel with certain elements, such as Mo and Ni, can change the material's resistance to sulfide stress cracking (SSC) [14–16] compared to the conventional MSS. SMSS demonstrates improved stress corrosion cracking (SCC) resistance. Moreover, the maximum service temperature has been raised from 150 to 175 °C. Monnot et al. [17] investigated the behavior of martensitic EN 1.4418 grade in hydrogen sulfide environments at pH below 4. They observed that EN 1.4418 grade demonstrates high corrosion resistance when the pH is 4 or above. However, the passive film layer properties of steel are compromised when the pH drops below 4. When the H_2S interacts with steel, it forms metallic sulfide and releases hydrogen, leading to hydrogen embrittlement and decreasing the mechanical strength of steel. It was also observed that the corrosion product layer of 40 microns formed at the surface of the EN 1.4418 grade steel. The SSC susceptibility of MSS in oil and gas production environments is linked to the chromium levels at the lower passivity limit. Due to the vulnerability, the modified SMSS forms were developed. These enhanced steels have a reduced carbon content (≤ 0.03%) and include additional alloying elements such as nickel, molybdenum, copper, and titanium which greatly improve the resistance of SMSS steels to sulfide stress cracking (SSC). These elements enhance the steel's resistance to localized corrosion, particularly in low pH environments, thereby improving its overall resistance to SSC [18]. The research focuses on MSS and SMSS and their role in the oil and gas industry. MSS is well-known for its corrosion resistance and mechanical toughness, which are accomplished by precision alloying and heat treatment methods. They are adaptable to both sweet and sour conditions, making them essential in present extraction processes. SMSS was designed to survive even more extreme conditions, such as high temperatures and corrosive environments with high chloride concentrations. SMSS has improved characteristics such as increased toughness, strength, and higher corrosion resistance, especially against sulfide stress cracking.

Figure 1 shows the schematic representation of environmental parameters and different types of environmentally induced cracking on MSS and SMSS.

Types of environmentally induced cracking and environmental parameters effecting MSS and SMSS

Passive film breakdown

Stainless steel's corrosion resistance is due to the formation of a protective oxide film on the surface, which is associated with the film's semiconducting properties. The semiconducting properties of the film will be impacted by its composition and structure. The passive oxide film has many point defects, including cation vacancies, oxygen vacancies, cation interstitials, and substitutional atoms. Plenty of research has indicated that the passive film of stainless steel (SS) consists primarily of chromium oxides, iron oxides, hydroxides, and iron compounds. On the other hand, the composition of the passive film varies with the pH of the solution and electrolyte for film formation. The degree of protection provided by the passive film is determined by the adhesion of the oxide film, its thickness, continuity, and coherence. In addition to this understanding, the diffusivity of metal and oxygen in the oxide film is very crucial.

The H_2S partial pressure effect

The level of hydrogen sulfide in the environment significantly impacts the severity and failure rate of sour corrosion. There are two ways in which the partial pressure of H_2S affects corrosion. First, it contributes to a drop

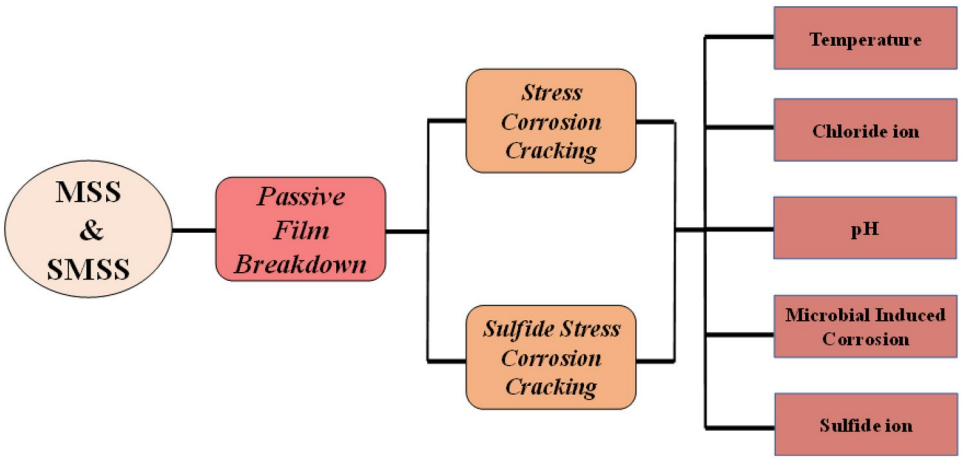

Fig. 1 Schematic representation showing environmental parameters and different types of environmentally induced cracking on MSS and SMSS

fall in pH and the potential for sulfide stress cracking, a form of hydrogen embrittlement, which are both caused by an increase in hydrogen sulfide partial pressure [19, 20]. Sulfides would be produced when hydrogen sulfide reacted with metal surfaces. These sulfides would promote the incorporation of hydrogen, which would lead to a local loss in mechanical behavior [12, 21]. SSC is the cracking of metal that involves corrosion and tensile stress (residual and/or applied) in the presence of H_2S and water phase. SSC can be managed and will not be a problem if the H_2S pressure is kept lower than 0.3 kPa [22]. The second method is H_2S partial pressure, which has a significant role in the features of the sulfide corrosion product layer that is formed. As H_2S levels increase, the corrosion film becomes less adherent and weaker, which reduces its contribution to the prevention of corrosion [23]. Liu et al. [24] investigated the SSCC behavior of two steels, 13Cr stainless steel and P110 steel, in a simulated acidic annular environment with H_2S/CO_2. The results showed that the steels exhibited different corrosion behaviors and susceptibility towards SSCC, with the 13Cr steel showing general corrosion and higher susceptibility towards SSCC in the H_2S/CO_2 environment and the P110 steel showing severe pitting and lower susceptibility towards SSCC. The presence of additional H_2S affected the corrosion of both steels, with the susceptibility towards SSCC being significantly increased by the increase in H_2S partial pressure. ISO15156 specifies the selection and qualification of corrosion-resistant alloys (CRAs) and other alloys for use in H_2S-containing oil and gas production and natural gas treatment plants. Restrictive application limits concerning temperature, partial pressure of H_2S, chlorides, pH, and elemental sulfur are specified in which MSS can be used safely and reduce the risk of SSCC. The established pH_2S limit for martensitic SS used for any equipment or component is a maximum of 10 kPa (1.5 psi) with no restriction on temperature and chloride.

The effect of pH

The pH has a significant impact on the composition of the corrosion product layer. pH measures the hydrogen ion concentration in an aqueous solution and is impacted by dissolved H_2S and CO_2. Temperature and salinity affect H_2S and CO_2 solubility. At low pH levels, the produced iron sulfide product is very soluble and does not precipitate on the surface of the steel. Iron sulfide coating develops and precipitates on the surface at higher pH values (pH = 3–5), preventing corrosion [25]. In ISO 15156–2, most MSS applications are qualified for a pH value of more than 3.5. The stability of the passive film at room temperature in the case of 13% Cr stainless steel depends on the concentration of chloride ions, the pH of the solution, and the partial pressure of H_2S. According to Marchebois et al. [26], the surface was active in the low pH (3.5) but showed nonstable passive behavior in the higher pH (4.0) environment. It is also observed that pitting causes the pH in the pit to drop, accelerating the penetration of hydrogen [27].

Effect of microbiologically influenced corrosion (MIC)

Microbial-induced corrosion is a type of corrosion that is induced/produced by the presence or action of microorganisms [28]. The microbial activities of these organisms can initiate both anodic and cathodic reactions in specific ways, and thus, corrosion is influenced significantly [29, 30]. Studies states that around 20% of corrosion is due to microbial activities [31]. The significant role of microorganisms in corrosion is seen in soils with less oxygen levels, high clay contents, low redox potentials, neutral pH values, and very poor drainage. These microorganisms can act as sole reason for corrosion and have no effect on corrosion, and also, they can act as corrosion inhibitors [32]. Identification of microbial corrosion using naked eye is challenging due to

the complications caused by conventional corrosion materials, deposits such as tubercles, and fouling.

The bacteria which are responsible for metal corrosion are classified as anaerobic or aerobic. These bacteria are of different kinds such as sulfate-reducing bacteria (SRB), iron-reducing bacteria (IRB), ion-oxidizing bacteria (IOB), and slim-forming bacteria [33]. MIC requires biofilm to grow on metal surfaces. Microorganisms are attached to metal surfaces, and during cell replication, extracellular polymeric substances are excreted. This leads to the formation of biofilms and thereby accelerates MIC. The stages of biofilm formation are shown in Fig. 2 [34]. Biofilms contribute to metal structural failure through the direct access of hydrogen ions produced by the cathodic reactions in metals by microorganisms, controlling the oxygen diffusion at the metal interface, which enhances the growth of anaerobic microorganisms, and creating a pathway for syntropic interactions that increase the growth of anaerobic microorganisms and the formation of inorganic and organic acids.

Effect of chloride concentration

The passivation film on stainless steel is known to drastically deteriorate when chloride ions are present in the formation water, especially at high temperatures. According to SSC studies performed by Kermani et al. [35] over a pH range of 3.5 to 5.5, low chloride content in condensed water environments performed better than higher chloride content, indicating that chloride content contributes to SSC more than pH alone. The electrical characteristics of passive films grown on SMSS in aqueous 0.6 NaCl solution and 2.1 M NaCl solutions with the addition of sodium acetate and acetic acid were studied by Soares et al. [36]. They found that, when compared to the NaCl/NaAc acid solution, the electrochemical behavior of SMSS in the 0.6 M NaCl solution exhibits the highest pitting potential and highest polarization resistance. According to their findings, the passive film of SMSS in an aqueous solution of NaCl is about three times higher than the oxide film generated in a NaCl/NaAc solution. For modified 13% Cr and 15% Cr stainless steels, Sunaba et al. [37] examined the impact of chloride ion concentration on passivation and corrosion product coatings in simulated formation water at high temperatures in a CO_2 atmosphere. Modified 13% Cr stainless steels at 150 °C had a more stable passivation layer due to the lower carbon content and the addition of nickel and molybdenum. The molybdenum concentration increased the corrosion product films' stability when exposed to high-temperature CO_2 and chloride. In comparison to 13% Cr stainless steel at 150 °C, modified 13% Cr-2% Mo stainless steel demonstrated good localized corrosion resistance. Wang et al. [38] studied the corrosion behavior of two types of super martensitic stainless steels (S-165 and HP) in a chloride environment using potentiodynamic polarization curves and electrochemical impedance spectroscopy. In Fig. 3a and b, potentiodynamic polarization curves were used to assess the corrosion behavior of S-165 and HP SMSS samples in solutions with varying concentrations of NaCl at 30 ℃. The results showed that when the polarization was above the pitting potential, there was a significant increase in the current density, indicating the initiation of pitting. Additionally, the pitting potential values decreased with increasing Cl^- concentrations for both types of SMSS, and a clear passive region was detectable. Corrosion resistance decreases as the environment becomes more aggressive. Understanding the behavior of SMSS in chloride-rich conditions is critical for predicting their stability and lifetime.

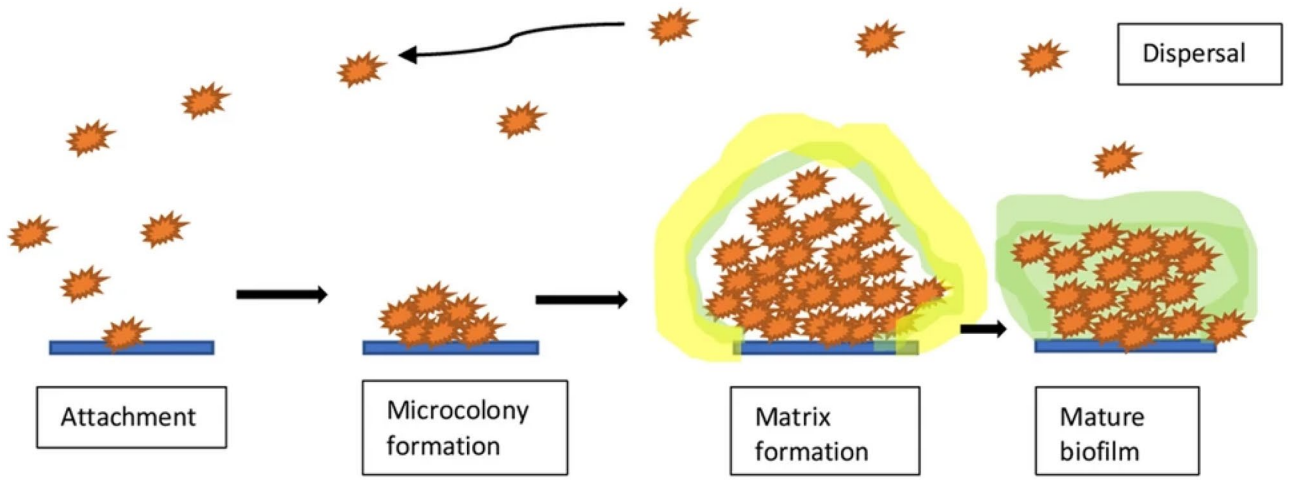

Fig. 2 Development of biofilm [34]

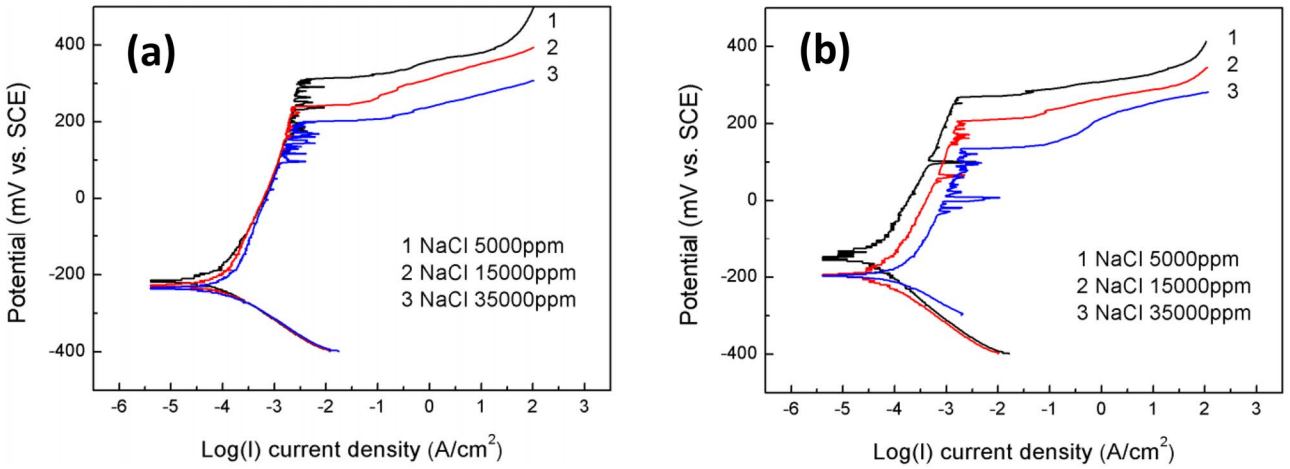

Fig. 3 **a** Potentiodynamic polarization curves of S-165 SMSS. **b** Potentiodynamic polarization curves of HP SMSS [38]

Stress corrosion cracking

Stress corrosion cracking (SCC) is principally regulated by the passive film's stability and the local chemistry. SCC can happen under several different conditions, such as a wide pH range (above depassivation pH) and the moderate-to-high temperatures needed for downhole applications. The mechanism of SCC mainly includes anodic dissolution, hydrogen embrittlement, and anodic dissolution + hydrogen embrittlement. Pitting corrosion is the primary cause of SCC (this requires confirmation). Figure 4 depicts the SCC mechanism of super 13Cr stainless steels during anodic polarization. The corrosion-resistant passive film could be easily formed on the surface of super 13Cr, martensitic stainless steel with a high Cr content, to protect the substrate, as illustrated in Fig. 4a. The passive film can be easily penetrated and

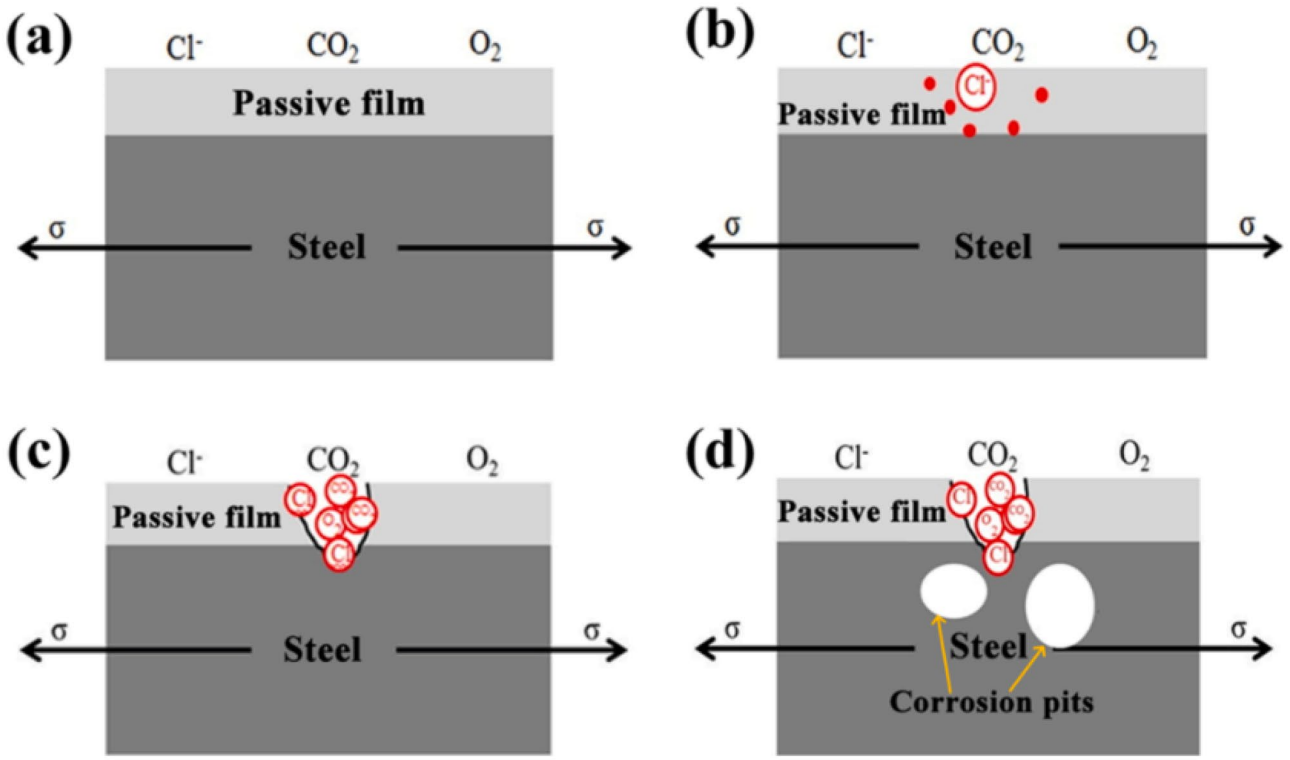

Fig. 4 SCC model of SS under anodic polarization [39]

ruptured because of the small radius of the chloride ion and its significant penetration ability, as shown in Fig. 4b. Following the formation of the small metal matrix and passive film form, pitting corrosion begins to form. The anode metal is continually dissolved under the chloride ions and CO_2, pitting nucleates and continuously expanding, as shown in Fig. 4c and d.

When cathodic polarization is employed, the SCC mechanism of 13Cr stainless steel is shown in Fig. 5. When the cathode is utilized in the corrosive environment of coexisting chloride and $CO_2 + O_2$, the following reaction occurs.

$$H_20 \rightarrow H^+ + OH^- \quad (1)$$

$$2H + 2e^- \rightarrow H_2 \quad (2)$$

$$CO_2 + H_2O \rightarrow H_2CO_3 \quad (3)$$

$$H_2CO_3 \rightarrow HCO_3^- + H^+ \quad (4)$$

$$H_2CO_3 \rightarrow CO_3^{2-} + H^+ \quad (5)$$

$$2H_30^+ + 2e^- \rightarrow 2H_20 + H_2 \quad (6)$$

Hydrogen atoms and H_2 can be produced from the H + that is formed during the cathodic process. The passive film can allow H_2 to pass through while the matrix absorbs it. H_2S poisons the reduction reaction of hydrogen atoms leading to penetration of the atom in the metal and the formation of entrapped hydrogen molecules. Figure 5a illustrates how H atoms can diffuse through a passive film's surface and move inside the substrate. The migrated H atoms will then pile up together at lattice gaps or defects. The accumulation of H^+ at a dislocation promotes dislocation emission and movement, resulting in the localization of stress/strain. The concentration of H^+ near the dislocation will stimulate emission and movement, leading to the legalization of stress and strain. Figure 5b shows how quickly cracks form when tensile stress is added, and the dislocation cumulative stress in the high-strain region is equal to the hydrogen-weakened atomic bond force. After the crack forms, the tensile stress applied to it causes hydrogen atoms to continually flow towards the fracture tip. As a result, the stress at the crack tip increases, which stimulates the rapid crack expansion and results in SCC, as illustrated in Fig. 5c.

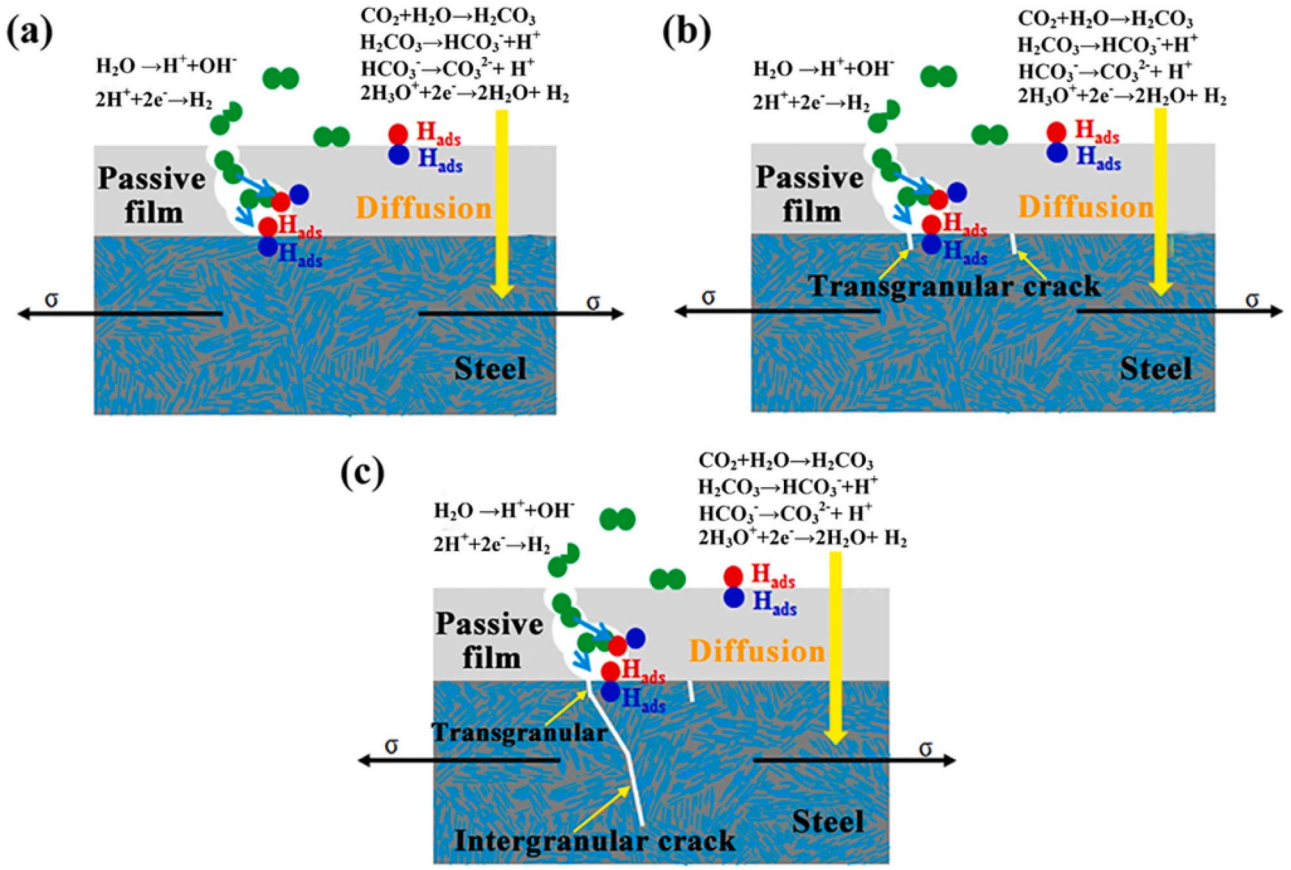

Fig. 5 SCC design in super 13Cr stainless steel with cathodic polarization [39]

Table 1 Heat-treated 13Cr MSS mechanical properties (AISI 410)

Tempering temperature (°C)	Yield strength (MPa)	Ultimate tensile strength (MPa)	Elongation (%)
400	673.70	778.95	8.30
500	648.32	686.57	9.10
600	658.34	865.73	6.50
650	405.86	598.33	9.90
700	358.10	518.57	11.10

Localized corrosion has been widely acknowledged to be a precursor of SCC. SCC can begin locally and develop when an alloy's corrosion potential exceeds its repassivation potential. SCC develops at potentials over E_{rp} for localized corrosion, and cracks grow at higher potentials. The corrosion potential (E_{corr}) is the potential naturally taken by the material in a tested medium [40]. The pitting potential (E_{pit}) is the potential at which pits start to be formed. The repassivation potential (E_{rp}) is the potential at which pits formed are repassivated. The length of the passive region between E_{corr} and E_{pit} shows the stability of the passive film and, consequently, the material's ability to resist pit formation. The relative position between E_{rp} and E_{corr} shows the repassivation capacity of the material, when the $E_{corr} - E_{rp} < 0$.

Modifying the chemical composition and heat treatment process of MSS can improve its mechanical properties and corrosion resistance. Steel microstructures and properties are greatly influenced by heat treatments. Mabruri et al. [41] proposed that 13Cr MSS be modified by adding Mo and Ni. They investigated the tensile properties of Mo and Ni under tempered conditions. They observed that adding 1% and 3% Mo increases the steels' tensile strength and elongation whereas adding 3% Ni decreases both of those qualities. Rusnaldy et al. [42] investigated the impact of tempering temperature on 13Cr MSS (AISI 410) to determine their susceptibility to SCC in a 3.5% NaCl solution. According to the procedure established by Nishimura et al. [43], SCC tests were performed on each heat-treated specimen at two distinct constant loads of 40% and 80% of the ultimate tensile strength (UTS) in a solution of 3.5% NaCl. The susceptibility of 13Cr MSS (AISI 410) was investigated under varied tempered conditions. Table 1 shows the impact of tempering temperature on the mechanical properties of 13Cr MSS.

It is evident that when the tempering temperature rises, the yield strength and ultimate tensile strength drop. For 240 h of SCC testing, steels that were tempered at a high tempering temperature did not fail. Figure 6 shows the fracture surfaces of specimens that have been tempered and continuously loaded with 80% of UTS. At 400, 600, and 650 °C, the fracture surfaces of tempered specimens were comparable

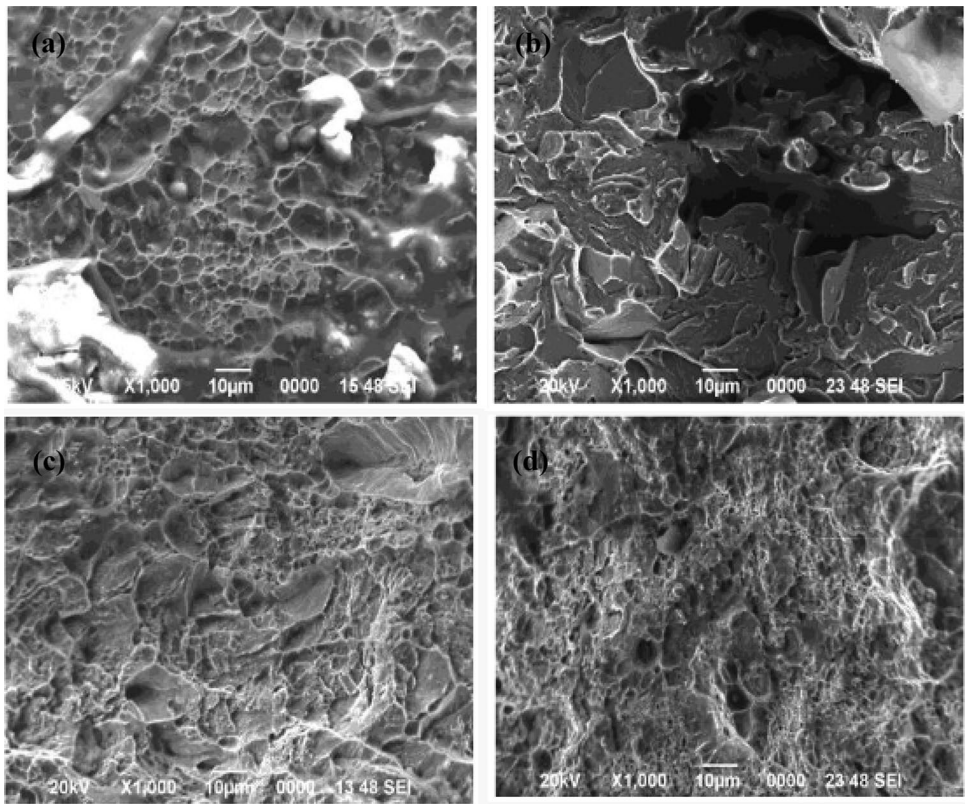

Fig. 6 The fracture surfaces for specimens that had been tempered at temperatures of **a** 400 °C, **b** 500 °C, **c** 600 °C, and **d** 650 °C under a continuous load of 80% of UTS [42]

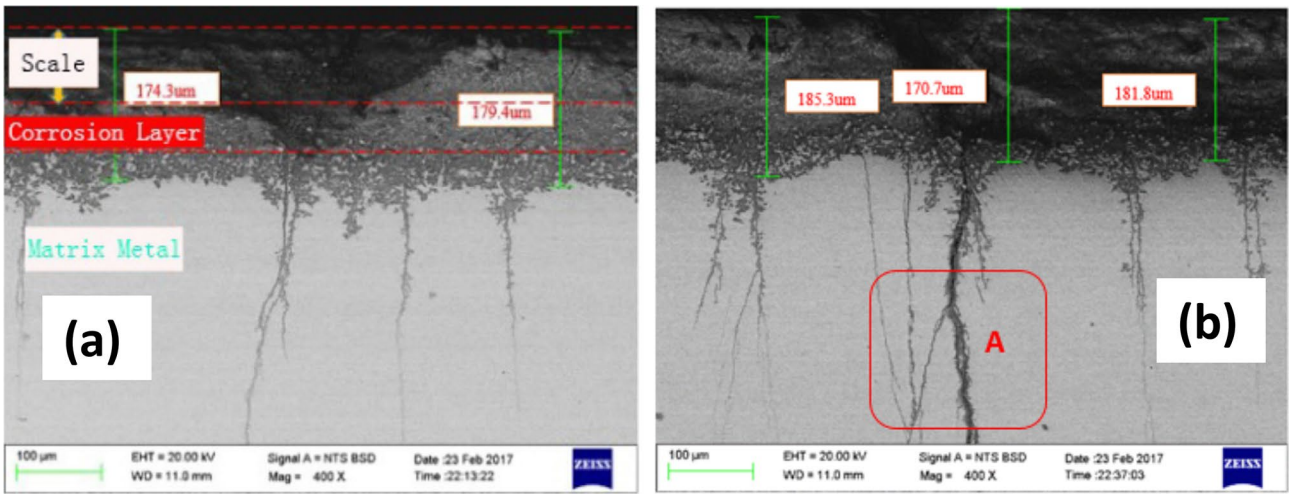

Fig. 7 Crack morphology analysis by SEM [44]

(see Fig. 6a–d). Intergranular cracks and dimple rupture fractures were present on the fracture surfaces, indicating ductile failure. At a tempering temperature of 500 °C, the fracture surface of steel exhibits fissures and cleavage fracture (see Fig. 6b). The study demonstrates the significance of optimizing tempering processes for the durability and performance of MSS in harsh environments and provides valuable recommendations for industrial applications.

The SCC evaluation of super 13Cr tubing in a deep gas well at a depth of about 7100 meters, under high-pressure conditions of 60 MPa and an average temperature of around 130 °C, was studied by Zhang et al. [44]. They used optical microscopy, SEM analysis, and EDS analysis to study the failed tube samples. There are numerous cracks from the exterior to the interior surface. Figure 7 shows SEM analysis of super 13Cr fracture morphology in a corrosion environment. The scale layer exhibits cracking, along with corrosion pitting where the scale has been removed. Most of the cracks were located where the corrosion pitting was beginning. It is feasible to conclude that the cracking of corrosion product films is what causes crack nucleation in a corrosion environment. This also demonstrates that the integrity of corrosion product films is crucial for crack nucleation in high-pressure and temperature environments, thereby enhancing the durability and operational safety of deep gas extraction tubing.

The high-temperature and high-pressure gas well of the Tarim Oilfield's S13Cr-110 oil pipe tubing has been repeatedly fractured in recent years. Failure incidents have led to huge financial losses. Ma et al. [45] used lateral comparison analysis of the failed tubing and an indoor simulation experiment to determine the cause of the tubing fracture. The study found various fracture types in couplings and pipe bodies, indicating failure mechanisms across wells. The fractures were primarily due to harsh operational conditions. They also proposed an effective solution to solve the fracture failure of the super 13Cr oil tubing. Figure 8

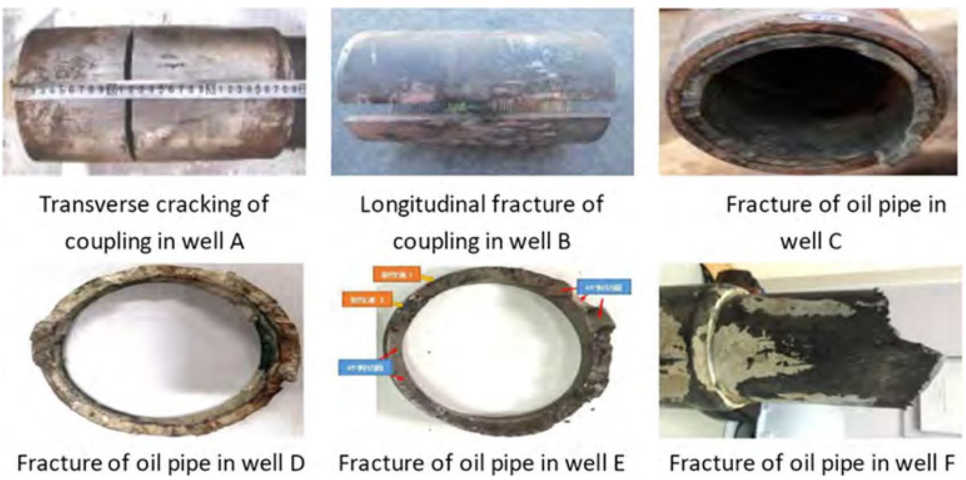

Fig. 8 Macroscopic appearance of failure oil pipes of six wells [45]

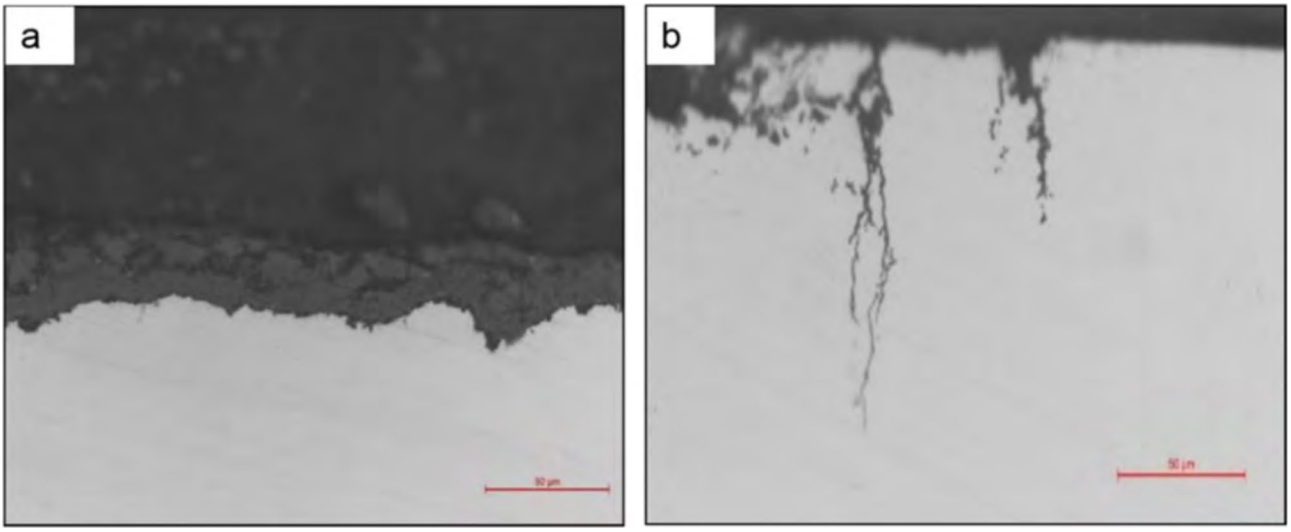

Fig. 9 Stress corrosion cracking test results of super 13Cr tubing in different completion fluids (**a** formate, **b** weight) [45]

shows the macroscopic morphology of the failed oil tubing of six wells.

The stress corrosion cracking test results of super 13Cr oil tubing in different completion fluids are shown in Fig. 9. The super 13Cr oil tubing is subjected to stress corrosion cracking in the phosphate contaminated with mud and oxygen, but no stress corrosion cracking crack is found in the formate contaminated with mud and oxygen. They observed that the stress corrosion cracking of the tubing's outer wall was the cause of the fracture. The leading cause of tubing fracture is a mismatch between the phosphate-based completion fluid, which is not resistant to mud and oxygen pollution, and the super 13Cr tubing. The study indicates that phosphate-based fluids in super 13Cr tubing environments can cause tubing failure due to SCC. They concluded that the format completion fluid is compatible with the super 13Cr oil pipe and that it successfully addresses fracture failure.

Compared to 13Cr stainless steel, 15Cr stainless steel, a relatively new form of MSS, has a higher content of Cr and Ni, which may enhance the material's resistance to corrosion. Zhao et al. [46] investigated the materials' environmental-assisted cracking susceptibility under stress and stress-free conditions, as well as the corrosion behavior of 15Cr MSS under applied stress. Under high temperatures and high pressure, they studied stress corrosion cracking using the immersion method. They noted that the 15Cr steel primarily experienced uniform corrosion, without any pitting or cracking, when the critical H_2S partial pressure was below 0.5 MPa,

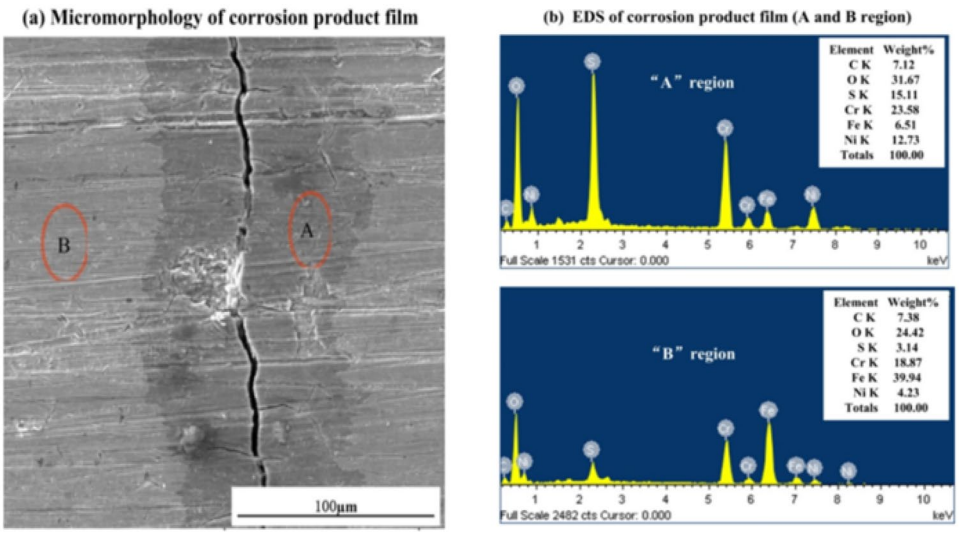

Fig. 10 Surface morphologies showing **a** corrosion products along the fracture in two distinct areas near the crack and **b** EDS analysis results

while the CO_2 partial pressure remained constant at 4 MPa, and the applied stress was 80 σs. However, when the critical H2S partial pressure was raised to 1 MPa and the test temperature was elevated to 150 °C, pitting and cracking sensitivity increased. Figure 10a shows the color differences between the corrosion products near the cracks (labeled as the "A" region) and the other no-cracking sections (labeled as the "B" region). The "A" region is dark gray, while the "B" region is lighter in hue. According to the results of the EDS analysis, which are presented in Fig. 10b, the "A" and "B" regions are primarily made up of several elements, i.e., sulfur, carbon, oxygen, and iron. The amount of sulfur found in the "A" region was significantly greater than that found in the "B" region. This implies that both H_2S adsorption on the active surface and anodic dissolution of the matrix contribute to the formation of stress cracking in the material. The increased sulfide concentration at the fracture site shows that H_2S can make the specimens more susceptible to cracking under stress.

Millet et al. [47] developed a new alloy with 16%Cr-4%Ni-3%Mo-1%Cu-0.5%V-Nb composition. New alloy material presents a higher ability to repassivate which gives a higher safety margin for the use of this material in this corrosive environment and higher corrosion potential, which will prevent hydrogen reduction. The material can, therefore, be used in high chloride solution up to 232 ℃ at 289 g/L NaCl in the presence of 0.2 bar of H_2S and 40 bars of CO_2 and up to 275 bars of CO_2 at 180 ℃ in a medium chloride environment. SCC and mass loss pp_{CO2}-T°C diagram is summarized in Fig. 11a. This mapping represents the different SCC and mass loss results obtained as a function of the CO_2 partial pressure and the test temperature. In high chloride content (NaCl above 150 g/l), SCC and mass loss tests show that the new alloy demonstrates higher corrosion resistance performance than Super 13Cr when temperatures are above 365 °F (185 °C), as illustrated in Fig. 11b.

Sulfide stress corrosion cracking

Pipelines and oilfield equipment/tubulars exposed to hydrogen sulfide are prone to sulfide stress corrosion cracking (SSCC). Sulfide stress corrosion cracking (SSCC) is a brittle failure by cracking under tensile stress and corrosion in the presence of water and H_2S. Several authors attribute the failures to hydrogen embrittlement caused by hydrogen sulfide [48, 49]. Hashizume and Inohara [50] studied the pH limit for depassivation of low-carbon 13Cr stainless steels with varying molybdenum contents (0–1.9 wt%) immersed in a 5% NaCl and 0.5% acetic acid solution. They suggested a relationship between metal chemical composition and depassivation pH. The result demonstrates that as molybdenum concentration increased, the steel's depassivation pH reduced. This is significant because the passive coating breaks and atomic hydrogen produced during the corrosion process can penetrate the steel when the pH of the solution is lower than the depassivation pH of the material. Therefore, a lower depassivation pH indicates strong SSC resistance. H_2S reacts with the metal to form metallic sulfides, releasing hydrogen that can be absorbed and reducing local mechanical characteristics. Passive film breakdown can also result in pitting, which can lead to crack propagation. Protons are formed, and the pH of stainless steel decreases during pitting corrosion due to the hydrolysis reaction of metallic ions at the initial pit. The decrease in pH prompts the dissolution of the metal within the initial pit. Sakamoto et al. [51] studied the effect of environmental factors on the SSCC property of the modified 13Cr stainless steel. They found that as the Cl^- level increased, the corrosion morphology altered from a passive state to either pitting or general corrosion, allowing hydrogen to enter the steel and resulting in SSC susceptibility. The findings demonstrate that the modified 13Cr SS has much greater SSC resistance than 13Cr SS. Ayagou

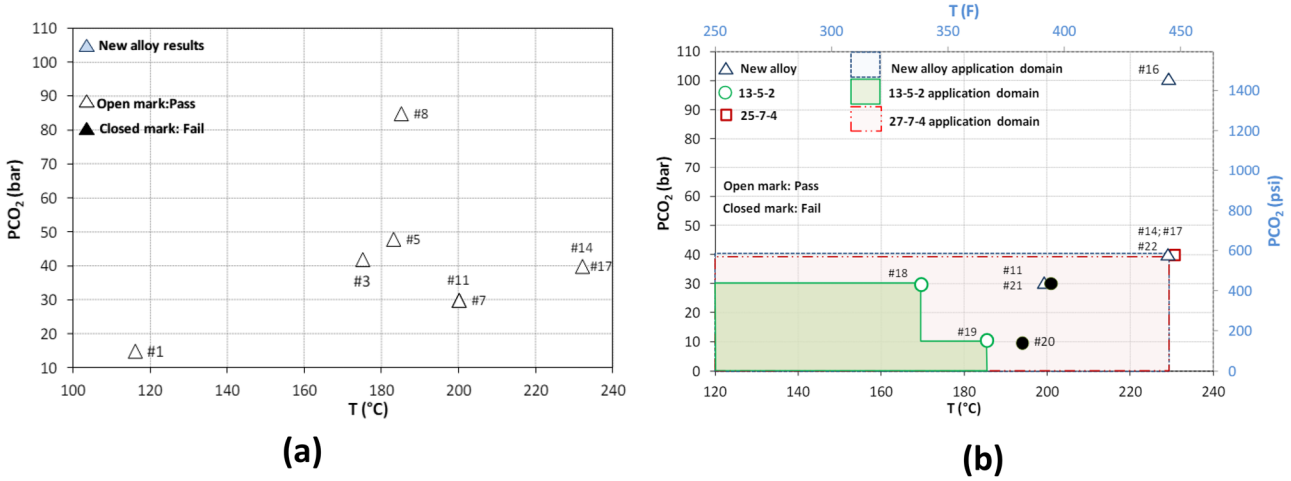

Fig. 11 **a** SCC $ppCO_2$-temperature mapping of new alloy material (medium and high chloride conditions). **b** The application domain of the new alloy compared to 13–5-2 and 25–7-4 in high chloride conditions

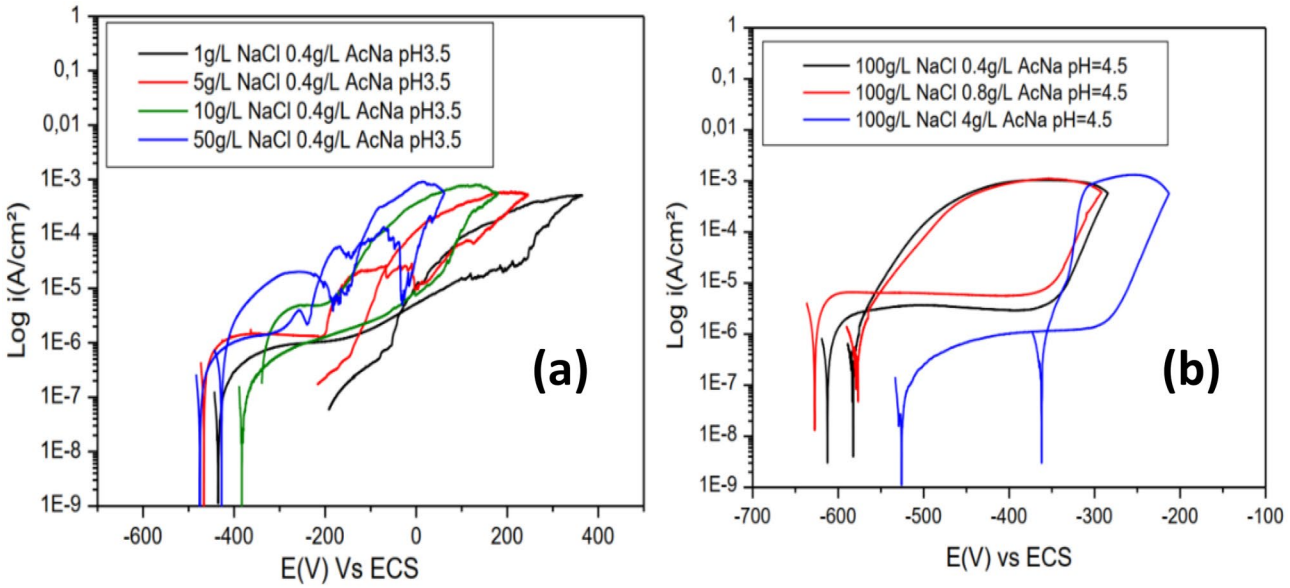

Fig. 12 **a** Cyclic potentiodynamic curves (pH = 3.5, 0.4 g/L CH_3COONa) with different NaCl content. **b** Cyclic potentiodynamic curves (pH = 4.5, 100 g/L NaCl) with different CH_3COONa content [52]

et al. [52] investigated the SSCC performance of an SMMS 110 ksi (13Cr-$_5$Ni-2Mo) using different methods: the NACE TM0177 method A uniaxial tensile test, a slow strain rate test (SSRT), and a ripple strain rate test (RSRT). Figure 12a shows the cyclic potentiodynamic polarization curve at pH 3.5 with 0.4 g/L CH_3COONa with different NaCl content at 24 °C with 0.1 bar H_2S in CO_2. It is clearly observed that by increasing chloride content, the pitting potential decreases as well as the passivation potential. Figure 12b shows that by increasing the acetate content, the curve is sifted into the more noble region, the passivity current density is reduced, and the passivation capacity is increased, which will form less pitting.

Table 2 compares the tested material's SSC performance with a uniaxial tensile test (NACE method A), SSRT, RSRT, and electrochemical analysis prediction. All conditions show a good correlation except for water formation conditions with high acetate concentration, where the material performs well based on electrochemical prediction and when tested with NACE method A but fails when tested with SSRT and RSRT.

Flores et al. [53] asses the H_2S limit of 13Cr$_4$Ni1Mo-110 ksi SMYS (758 MPa) material which is used by Petroleum Development Oman (PDO) in gas/condensate wells at high-pressure high-temperature conditions. The susceptibility of 13Cr4Ni1Mo-110 was tested, by the NACE TM0177 C-ring tests conducted at different temperature ranges (25 to 120 ℃), H_2S partial pressure (2.5 to 10 mbar), 20 bar CO_2, and at a chloride content of 20,000, 100,000 and 175,000 mg/L. The 13Cr4Ni1Mo material is susceptible to SSC at ppH_2S values as low as 2.5 mbar, even at 40 °C and pH is 4.0. If the chloride concentration is lowered to 100,000 mg/L and the pH value is 4.0, the material was found to be resistant to SSC. The results show that 13Cr$_4$Ni1Mo material is susceptible to SSCC in an environment with a low amount of H_2S at a lower temperature of around 40 ℃. At higher temperatures (2.5 mbar H_2S, 65 ℃,

Table 2 SSC correlation across different testing techniques [52]

Test condition	Electrochemical prediction	SSRT	RSRT	NACE A	Correlation
1 g/L NaCl, 0.4 g/L AcNa, pH = 3, 1% H_2S/CO_2	Pass	Pass	Pass	Pass	Good correlation
50 g/L NaCl, 0.4 g/L AcNa, pH = 3, 1% H_2S/CO_2	Fail	Fail	Fail	Fail	Good correlation
5 g/L NaCl, 0.4 g/L AcNa, pH = 3.5, 1% H_2S/CO_2	Pass	Pass	Pass	Pass	Good correlation
100 g/L NaCl, 0.4 g/L AcNa, pH = 4.5, 10% H_2S/CO_2	Fail	Fail	Fail	Fail	Good correlation
100 g/L NaCl, 4 g/L AcNa, pH = 4.5, 10% H_2S/CO_2	Pass	Fail	Fail	Pass	Not good

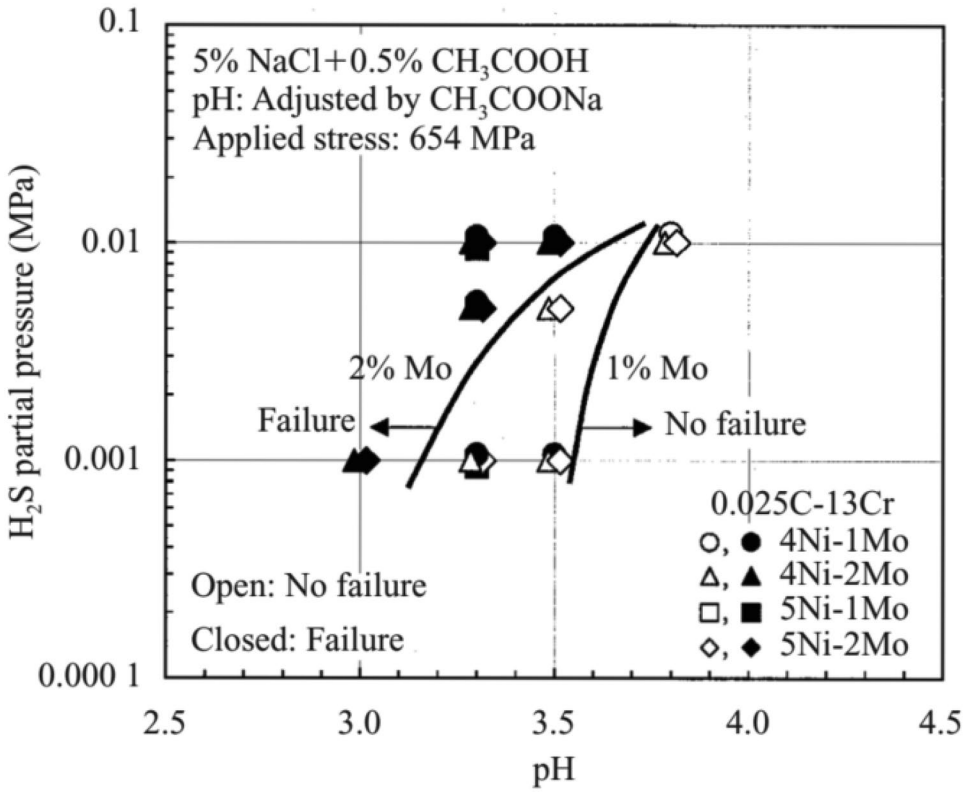

Fig. 13 Ni and Mo impacts on SSC resistance of 0.025C-13Cr stainless steel [54]

100,000 mg/L chlorides, and pH 4.0), only localized corrosion was found but not cracking.

Molybdenum-containing martensitic 13Cr stainless steels are often used as production pipelines for sweet and mild sour producer wells because molybdenum improves the passive film's stability and pitting corrosion and SSCC resistance and they do not corrode easily when exposed to CO_2. Figure 15 shows the effect of Ni and Mo on the SSC resistance [54]. As Mo concentration increases from 1 to 2%, it moves the boundary of SSC occurrence towards low pH and high H_2S partial pressure or to a severe environment. However, the increase in Ni content does not affect the test results, as shown in Fig. 13.

The composition range of these stainless steels is defined by the UNS numbers S41425, S41426, and S41427. These numbers correspond to the so-called modified grades with specified minimum yield strengths (SMYS) between 95 and 125 ksi and Mo contents between 1 and 3 wt%. Above 3%, molybdenum precipitates with iron to form Fe_2Mo, lowering the corrosion resistance of the alloy. Monnot et al. [55] investigated the role of molybdenum content on the sulfide stress corrosion resistance of SMSS in a sour medium at room temperature. They performed the anodic polarization test in NACE B solution at pH 3.5 for a different amount of molybdenum (0.8, 1.5, 2.25, and 3.5) as shown in Fig. 14a. It is observed that as molybdenum content increases from 2.25 to 3.35, the corrosion resistance is significantly improved.

To determine the impact of excess molybdenum on SSC resistance, static SSCC tests on proof rings were performed. The time to failure for various Mo contents is depicted in Fig. 14b. The performance of the material was enhanced by adding molybdenum content. The specimens were free of corrosion and had a time to failure of 2.25 Mo of 705 h, which was barely below the acceptable level. The 3.5 Mo steel grade did not fail over prolonged exposures of up to 1000 h, showing that this steel grade is appropriate for usage in sour environments because it passed the SCC time-to-failure criterion. One of the most well-populated usage domains was presented by Takabe et al. [56] where several acceptable and unacceptable application envelopes were presented as pH-pH_2S plots at various discreet chloride concentrations; an example of the domain plot for high chloride concentration is provided in Fig. 15. By mapping out these application envelopes, the study provides valuable insights into the critical factors influencing the corrosion resistance of SMSS and aids in the selection of appropriate materials for specific operating conditions.

Millet et al. [47] developed the new alloy (16%Cr-4%Ni-3%Mo-1%Cu-0.5%V-Nb) for HPHT application and compared it with the SSC behavior and pitting resistance of the 13–5-2 SMSS. They observed that in medium chloride conditions, the new alloy presents a higher ability to repassivate as compared to the 13–5-2 material, which means that the material can be self-repaired in each environment. It is also

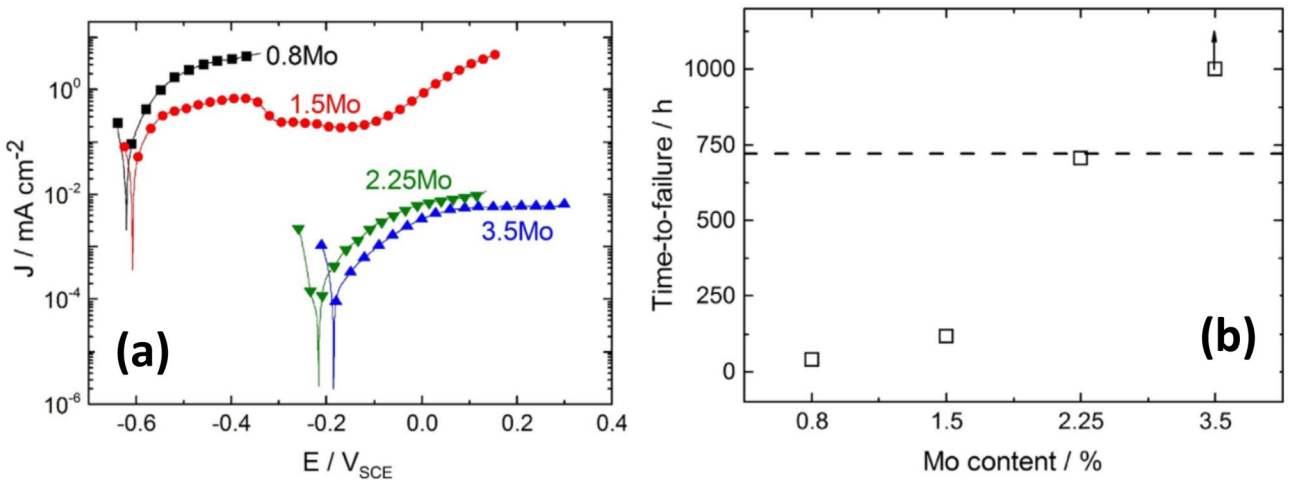

Fig. 14 **a** Polarization curves of laboratory temperature after 4 h of exposure at "25 °C" in NACE B solution. **b** Different steel grades' time-to-failure rings in NACE B solution [55]

observed that at higher chloride conditions, the new alloy presents higher pitting resistance which will lower the risk of hydrogen reduction. However, the 13–5-2 materials pitting resistance is lower, which will increase the risk of hydrogen embrittlement and crack propagation. They also observed that the new alloy slightly improves SSC performance compared to 13–5-2 material due to higher pitting corrosion resistance and the ability of the material to repassivate in the corrosive environment. Oliveira et al. [40] analyzed the SSCC performance of S13Cr-110 ksi grade stability in a specific reservoir environment with different pH (9 from 3.0 to 6.0), ppH_2S (from 0.01 to 0.1 bar) and NaCl content from 1 to 200 g/L) in a different condition such as shut in and flowing condition at both the wellhead and downhole location. The SSCC result shows that at higher chloride content, there is a significant influence on corrosion behavior. The reduction in ppH_2S from 0.03 to 0.02 bar does not lead to a significant change in the $E_{corr} - E_{rp}$ factor, which is 104 and

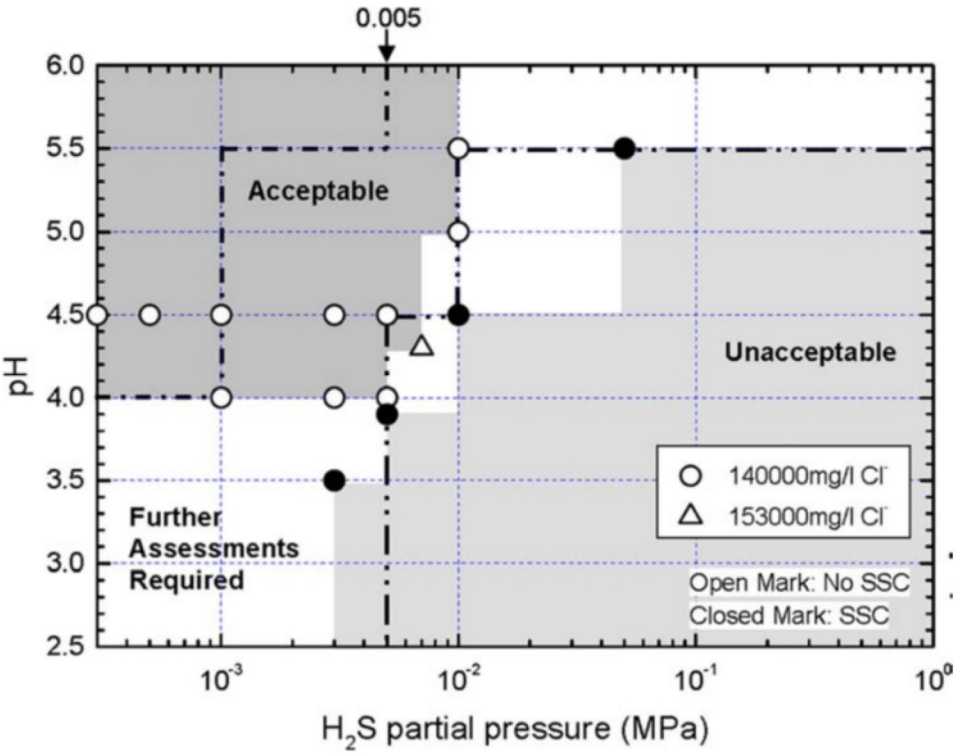

Fig. 15 SSC domain diagram of 110 ksi strength grade super 13Cr steel at 140,000 mg/L $Cl.^{-}$. From Takabe et al. [56]

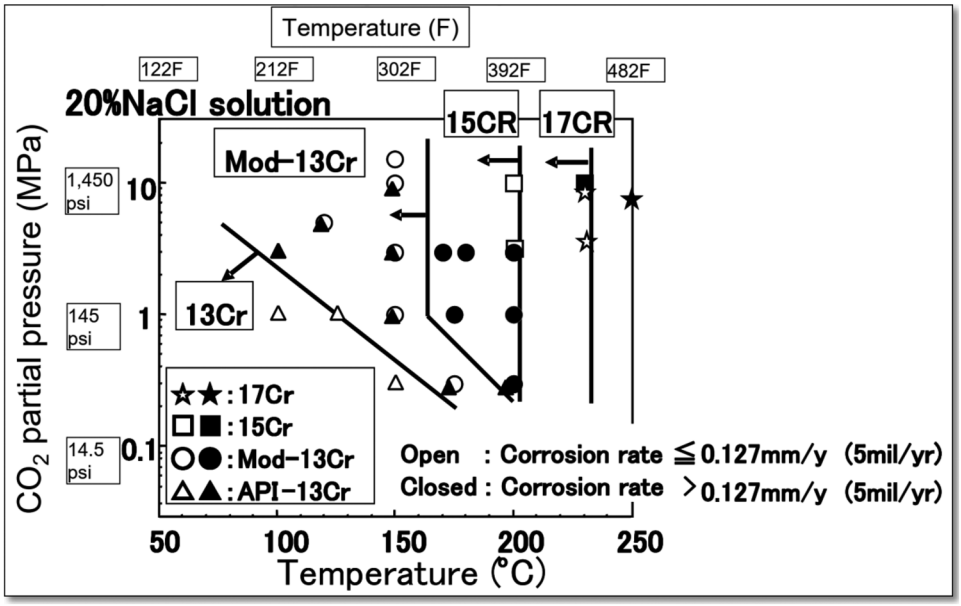

Fig. 16 CO_2 corrosion resistance map in 20% NaCl solution plotted as CO_2 partial pressure and the temperature in API-13Cr, Mod-13Cr, 15Cr, and 17Cr [57]

92, respectively. They observed that increasing the Cr and Mo content will improve the formation and stabilization of the passive layer against pitting corrosion.

In an H_2S environment with 100% specified minimum yield strength (SMYS) applied stress, Ishiguro et al. [57] reported that 15Cr and 17Cr have better performances in corrosion properties and mechanical properties than conventional martensitic stainless steel. Figure 16 shows the CO_2 corrosion rate map in API-13Cr, Mod-13Cr, 15Cr, and 17Cr under the corrosion environment of 20% NaCl solution as parameters of CO_2 partial pressure and temperature: the former one is 0.3 to around 10 MPa, and the latter one is 100 to 250 °C. The good samples are marked as open symbols, and the bad ones are marked as solid symbols. The corrosion rate is improved in the order of API-13Cr, Mod-13Cr, 15Cr, and 17Cr, which are arranged as Cr addition and corrosion-related alloy element addition. When the application limits are compared under 20% NaCl solution at 10 MPa of CO_2 partial pressure without any H_2S gas, Mod-13Cr, 15Cr, and 17Cr are 165 °C, 200 °C, and 230 °C, respectively.

Figure 17a–c for 15Cr-125 ksi grade, 17Cr-125 ksi grade, and 17Cr-110 ksi grade, respectively, shows the SSC resistance data. As depicted in Fig. 17a, when the chloride ion is smaller in corrosion conditions, the applicable limit in 15Cr-125 ksi grade is enlarged to a lower pH and a greater partial pressure of the H_2S region. SSC was not noticed in pH 3.5 and 0.1 MPa of H_2S at 1000 ppm chloride (=0.165% NaCl solution). Figure 17b compares SSC resistance for 17Cr-125 ksi grade to 15Cr-125 ksi grade. Although the application limit is increasing and 17Cr-125 ksi grade performs better in SSC than 15Cr-125 ksi grade, the SSC test is still being conducted to establish the SSC's upper limit. Figure 17c in the 17Cr-110 ksi grade illustrates SSC performance under three distinct chloride ion situations. The application limit is increased to a lower pH or a greater partial pressure of H_2S when the chloride ion is smaller.

Due to the addition of alloy elements, including Cr, Ni, Mo, Cu, and W, the passivation film's stability has enhanced, improving corrosion resistance. Duplex stainless steels have higher corrosion-resistant properties than 15Cr and 17Cr, but it may be possible to use 15Cr and 17Cr in a region that is more susceptible to milder corrosion in a duplex-targeting environment, in addition to their use as the higher grade of Mod-13Cr and API-13Cr in terms of corrosion-resistant properties and mechanical properties, particularly yield strength.

Role of microstructure

Martensitic stainless steels undergo a standard heat treatment process consisting of annealing, austenitizing, quenching, and tempering to achieve a desired combination of properties [58, 59]. The final microstructure is heavily influenced by the specific heat treatment applied and typically consists of martensite, undissolved and/or re-precipitated carbides, and retained austenite. The volume fraction and size of carbide particles, along with the amount of retained austenite, are critical factors that determine the steel's hardness, strength, toughness, corrosion resistance, and wear resistance. The quenching and tempering process improves stainless steel hardness by converting austenite to martensite. The austenitizing temperature influences not only the hardness of the steel but also its toughness and ductility. After quenching, the material is tempered to increase toughness. Kimura

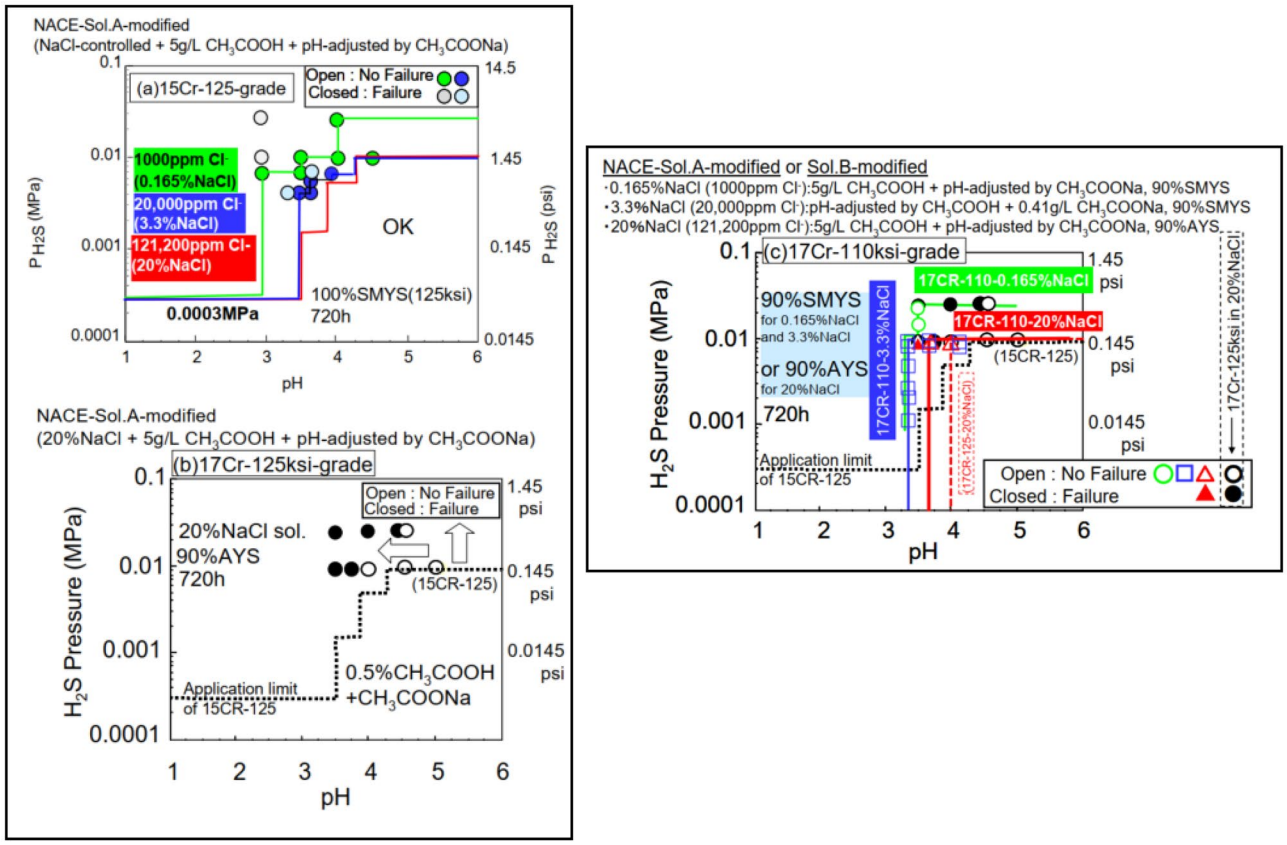

Fig. 17 SSC maps in **a** 15Cr-125 ksi grade, **b** 17Cr-125 ksi grade, and **c** 17Cr-110 ksi grade [57]

et al. [60] conducted a study to investigate the impact of the amount of retained austenite on the corrosion rate and susceptibility to pitting of modified 13Cr steel. They varied the amount of retained austenite between 3 and 40% by quenching and tempering the steel. The study found that retained austenite had a minor positive effect on the SSC resistance of the steel, despite being perceived as a potential weak point in steel structures due to its lower hardness and strength compared to martensite. The researchers hypothesized that this effect could be due to the slower diffusion of hydrogen in austenite compared to martensite, which could help reduce hydrogen embrittlement, a common cause of SSC in steel. They concluded that the microstructure of steel can affect its corrosion resistance and other properties. Zou et al. [61] observed that by introducing reversed austenite into the lath martensite matrix of a 13Cr-4Ni-1Mo martensitic stainless steel, it was possible to achieve a material with high tensile strength (905 MPa), yield strength (832 MPa), and elongation (18%). Moreover, they conducted slow strain rate testing on the specimens that had been electrochemically charged with hydrogen, and the results indicated that the addition of reversed austenite improved the steel's resistance to hydrogen embrittlement (HE). Figure 18 shows the microstructures achieved at different temperatures following the tempering of a specific material. As the temperature increases from 350 to 600 ℃, the size and distribution of the carbides change. The material goes from having predominantly intragranular carbides to predominantly intergranular carbides. The hardness of the material decreases as the size of the carbides increases. Intragranular precipitation of (Fe, Cr) 3C removes carbon from the matrix, reducing hardness and restoring a degree of ductility. Local variations in the Cr concentration are observed where intragranular carbides used to be located.

The austenitizing process can result in a variety of changes that can affect the corrosion behavior of steel. The dissolution of chrome carbides is one of these changes, which can increase the amount of dissolved chromium and carbon in the material. While a higher chromium content can lead to the formation of a more chrome-rich passive layer, improving corrosion resistance, higher carbon content can cause lattice distortion, resulting in a more defect-prone passive layer. Austenitizing stainless steel changes its microstructure by releasing chromium from carbides into the alloy matrix, releasing carbon into the alloy matrix, and increasing grain size. It is possible to achieve a martensitic

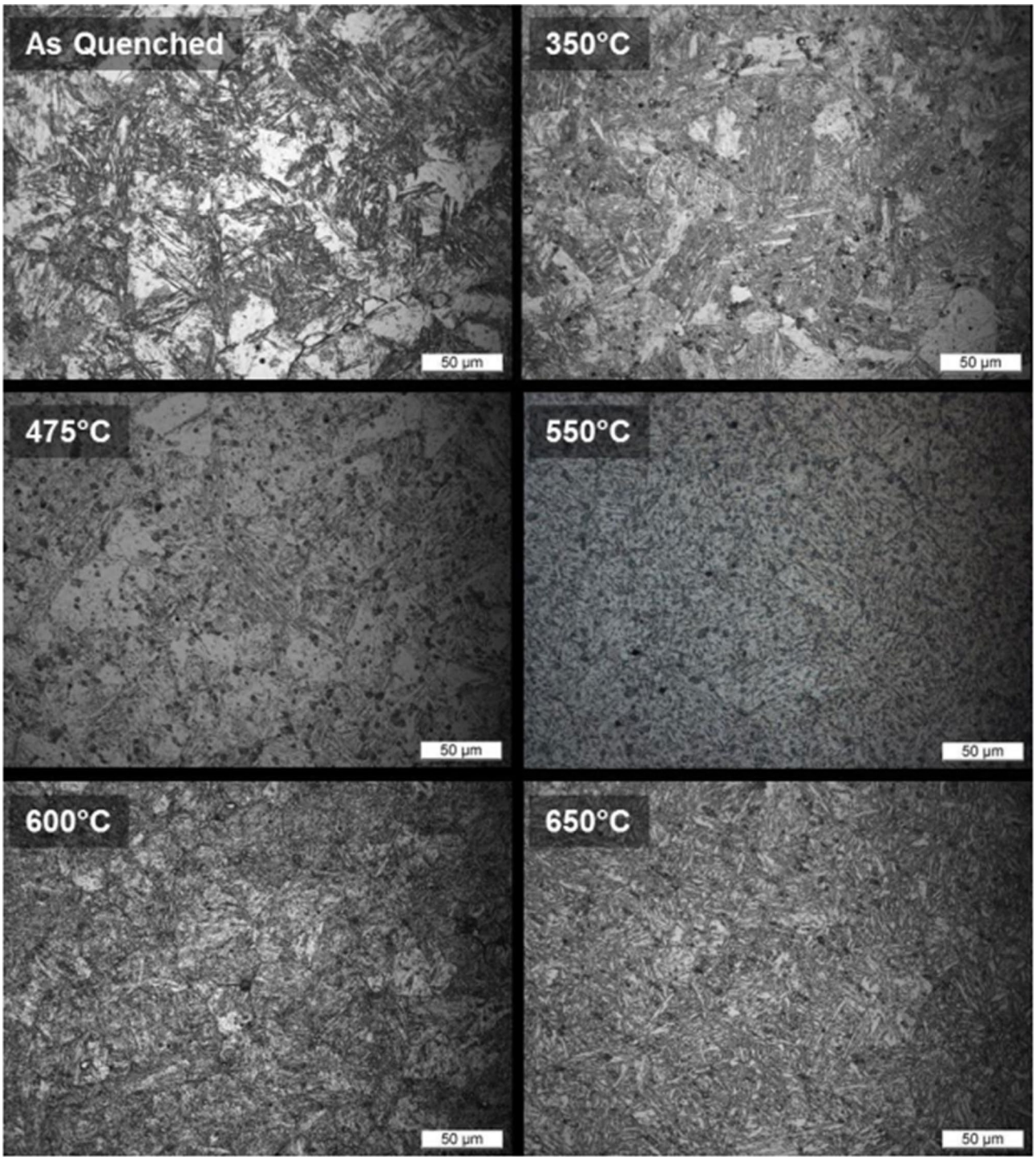

Fig. 18 Optical micrographs of 12% Cr stainless steel samples tempered after different tempering treatments, including the as-quenched condition [62]

microstructure with a significant increase in hardness by selecting the appropriate cooling phase after austenitizing. The release of chromium from carbides can improve stainless steel's passive behavior by providing more chromium for the formation of a chrome-rich passive layer. Carbon release, on the other hand, can have a negative impact on passive behavior due to the potential for high carbon content to cause internal lattice stress.

Bösing et al. [63] investigated the effects of austenitizing on the passive layer of martensitic stainless steel using

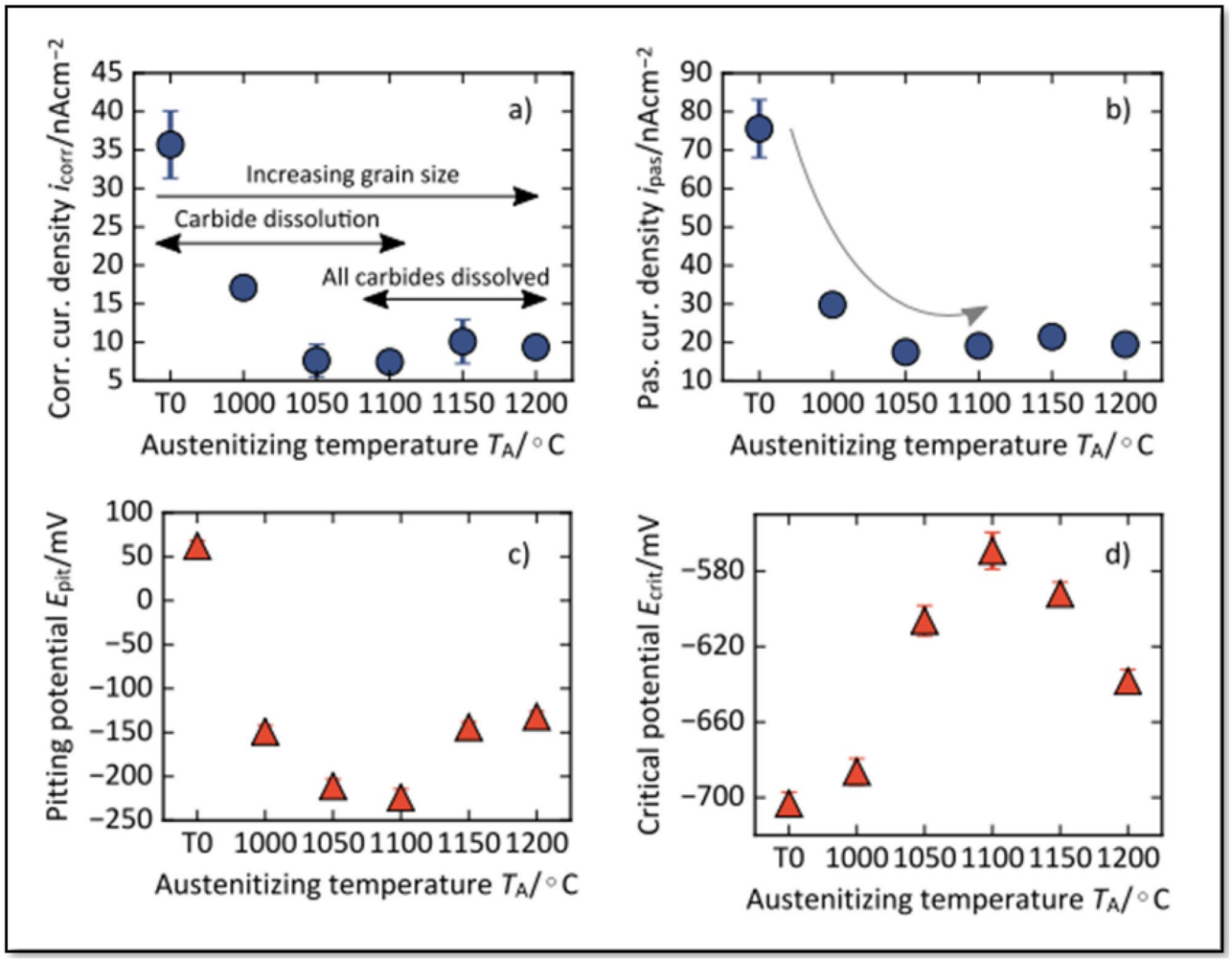

Fig. 19 Dependencies of different corrosion parameters on the heat treatment. **a** Corrosion current density, **b** passive current density, **c** pitting potential, and **d** critical potential [63]

different electrochemical measurement techniques. Figure 19a shows the corrosion current density at − 300 mV plotted against the austenitizing temperatures. The results showed that as the austenitizing temperature and chromium content increased, the corrosion current density, icor, decreased. The corrosion current density decreases slightly at austenitizing temperatures above 1100 ℃, which may be due to increasing grain size. The passive current density followed a similar pattern, as shown in Fig. 19b. Reduced corrosion current and passive current both indicate improved passivation against general corrosion. As the austenitizing temperature rises, the alloy matrix contains more chromium, which improves the steel's resistance to general corrosion. However, the pitting potential, E_{pit}, which represents the potential for stable pit growth, decreases with increasing austenitizing temperature (up to 1100 ℃), indicating a greater susceptibility to pitting corrosion (Fig. 19c). The potential increases as the austenitizing temperature rises further. However, the critical potential E_{crit}, which represents the potential at which a critical current density is exceeded, increases with increasing austenitizing temperature (as shown in Fig. 19d). This suggests that the corrosion rate is higher if pitting occurs at higher austenitizing temperatures. Interestingly, E_{crit} decreases again at austenitizing temperatures above 1100 ℃.

Increasing the austenitizing temperature of stainless steel to 1100 °C results in increased resistance to general corrosion due to carbide dissolution and subsequent chromium increase in the alloy matrix. This improves passivation and results in a thicker chromium-rich inner passive layer. However, raising the temperature above this point has no effect on the chromium content and does not improve resistance to general corrosion. While raising the austenitizing temperature to 1100 ℃ increases the chromium content in the alloy matrix, it also increases the carbon content, which causes internal lattice stress and results in a more defective passive

layer. As a result, raising the temperature above 1100 ℃ reduces resistance to pitting corrosion. Increasing the temperature, on the other hand, has no effect on the carbon content but does affect the grain size. Increased grain size reduces the density of lattice defects in the bulk material, resulting in a less defective passive layer and better resistance to pitting corrosion. Mesquita et al. [14] investigated the heat treatment on the pitting and sulfide stress cracking on the different grades of martensitic stainless steel (1.4542 and 1.4418 SS).

Mechanism of passive layer breakdown

Pitting corrosion is a common issue for most stainless steel, prompting extensive research into understanding its mechanism and finding effective protection methods. The corrosion induced by chloride ions (Cl^-) on certain metals and alloys occurs spontaneously due to factors such as the concentration and temperature of hydrated Cl^-, as well as the composition, type, and microstructure of the alloy. While debates persist regarding the precise mechanisms of pitting, it is generally accepted that it begins with localized breakdown of the protective barrier layer due to specific interactions with corrosive ions in the environment. Failure of this layer typically happens at sites on the metal surface with high cation vacancy diffusivity, often associated with structural irregularities at the interface of the barrier layer and inclusions like MnS and $Cr_{23}C_6$ precipitates. Once the protective layer is compromised, the underlying metal becomes susceptible to dissolution in that area, leading to the formation of pits with varying shapes. The composition and structure of the protective layer play a crucial role in this process, driving efforts to enhance its performance and reduce stainless steel's vulnerability to pitting corrosion.

Interestingly, Zhang and colleagues [64] explored the role of hydrated chloride ions in disrupting the passivity of $FeCr_{15}Ni_{15}$ single crystal through a combination of

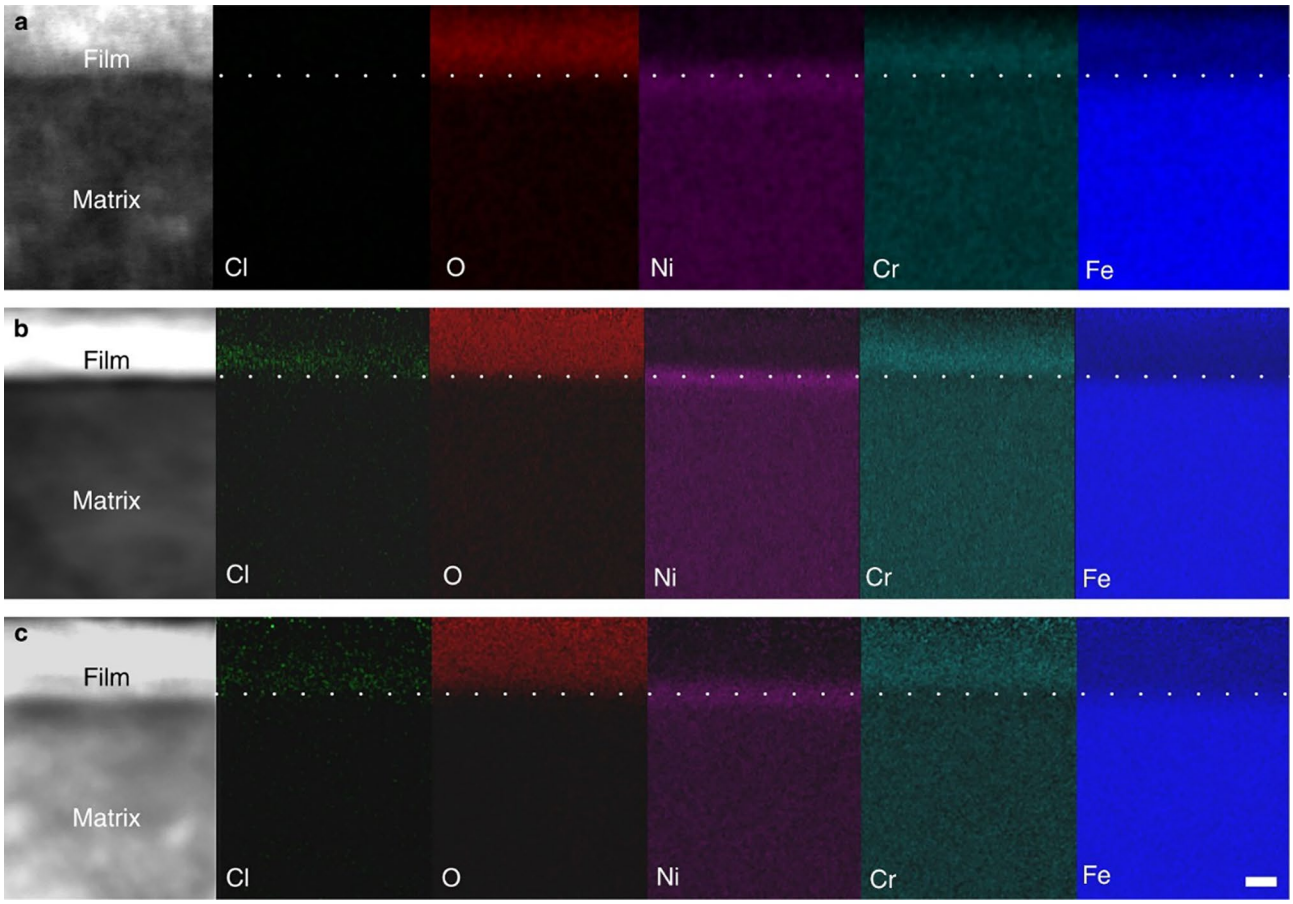

Fig. 20 Super-X EDS mapping illustrates the incorporation and penetration of chloride ions into the passive film, with accumulation observed at the interface between the matrix and the passive film. Element maps depict the formation of the film under various conditions: **a** in a 0.5 mol L^{-1} H_2SO_4 electrolyte at 640 mV/SHE for 30 min, **b** in a mixture of 0.5 mol L^{-1} H_2SO^4 and 0.3 mol L^{-1} NaCl electrolyte at 640 mV/SHE for 30 min, and **c** passivated in 0.5 mol $L.^{-1}$ H_2SO_4 electrolyte at 640 mV/SHE for 30 min followed by the addition of NaCl. The scale bars in **a** to **c** represent 2 nm [64]

experimental analysis and computational modeling (see Fig. 20). They suggested that certain grain boundaries between the amorphous region of the passive layer and nanocrystals facilitate the transport of chloride ions, causing disturbances in both the outer and inner layers. This disruption is thought to occur predominantly at specific weakened locations, where chloride species have less influence. Interestingly, these findings challenge the conventional notion that the point of weakest resistance to breakdown corresponds to areas with the highest chloride ion concentration; instead, it tends to occur in neighboring regions with diminished chloride ion influence.

On the other hand, the point defect model (PDM) suggests that corrosive halide species such as bromide, fluoride, iodide, and chloride infiltrate oxygen vacancies within the barrier film, resulting in the formation of cation vacancies at the interface between the barrier layer and the solution. This mechanism promotes the movement of cation vacancies through the passive film towards the interface between the metal and the barrier layer, as depicted in Fig. 21.

It should be noted that "*jm*" denotes the annihilation rate of $V_M^{x\prime}$ at the metal/barrier layer interface (m/bl). However, "*x*" represents the oxidation number of the host cation within the barrier layer. When $j_{ca} > j_m$, the cation vacancies on the cation sublattice of the barrier layer ($V_M^{x\prime}$) become localized at the m/bl interface. Consequently, at a specific concentration of cation vacancies, the barrier layer becomes detached from the base metal, resulting in the formation of a blister due to the remaining barrier layer. Subsequently, the barrier layer is unable to expand onto the metal surface, leading to the generation of V_o as indicated in the subsequent reaction:

$$\mathrm{m} \rightarrow \mathrm{M_M} + \frac{\mathrm{x}}{2}\mathrm{V_{\ddot{o}}} + \mathrm{x}e'$$

The resulting oxygen vacancies $V_o^{\cdot\cdot}$ can react autocatalytically with additional Cl^- species at the bl/electrolyte interface, thereby producing more oxygen and cation vacancies. These newly generated cation vacancies may migrate to the MMSS/bl interface and gradually accumulate, causing the separation of the passive layer and the occurrence of breakdown at the most susceptible locations with the highest diffusivities for cation vacancies.

Shahryari et al. [66] indicated that 316LVM stainless steel's susceptibility to pitting corrosion is strongly influenced by its crystallographic orientation. They found that specific crystallographic planes, such as {1 1 1} and {1 0 0}, exhibit greater resistance to pitting corrosion compared to planes with lower atomic density. This underscores the material's anisotropic nature in pitting initiation and stresses the importance of controlling material texture to improve

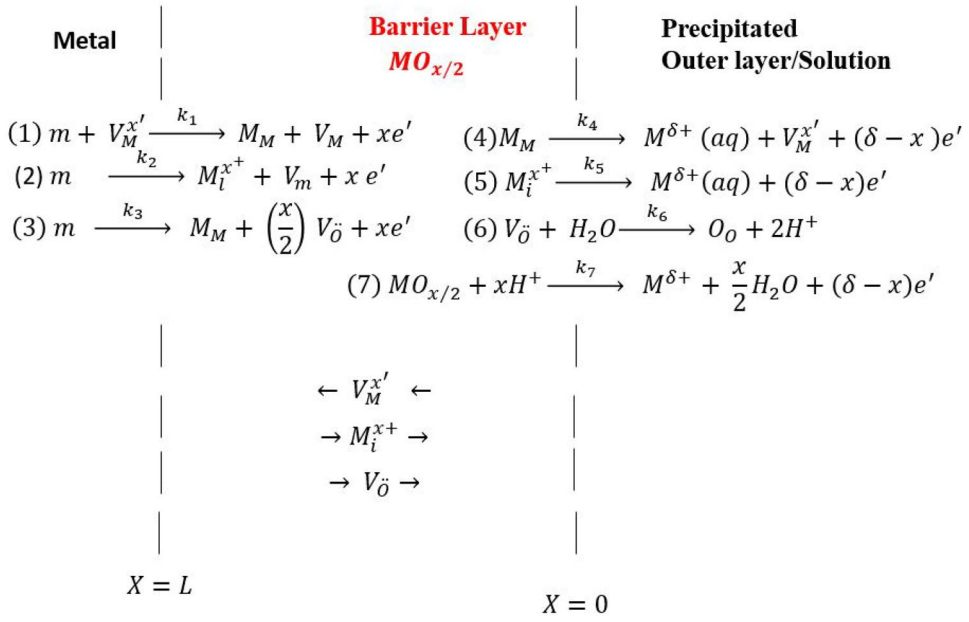

Fig. 21 Outline of the defect generation and elimination reactions suggested to occur at the interfaces of the barrier oxide layer on a metal, as proposed by the PDM. In this context, *m* and $V_M^{x\prime}$ represent the metal atom and cation vacancy on the cation sublattice of the barrier layer, respectively. M_i^{x+} is a cation interstitial, $V_O^{\cdot\cdot}$ is an oxygen (anion) vacancy,$M^{\delta+}(aq)$ is a cation in outer layer/solution interface, and M_M and V_m are the metal cation on the cation sublattice of the barrier layer and a vacancy in the modified martensitic stainless steel (MMSS) sample, respectively. O_O is an oxide ion in anion site on the anion sublattice, $MO_{x/2}$ is the stoichiometric barrier layer oxide. It should be noted that the point of reference for the coordinate system is the barrier layer/solution (bl/s) interface; hence, the flux of oxygen vacancies is represented as negative [65]

resistance against pitting. By employing generalized spherical harmonic functions to characterize pitting susceptibility and analyzing pit densities across different crystallographic planes, researchers can forecast and enhance the material's pitting resistance based on texture assessments. Consequently, optimizing material texture emerges as a novel strategy for bolstering the pitting resistance of SS316LVM stainless steel.

Numerous researchers have posited dielectric breakdown as the pivotal phase in elucidating the breakdown mechanism of the film. At the onset, the infiltration or adsorption of Cl^- ions emerges as the crucial initial step in this intricate process, as indicated by various studies [67–69]. Hoar and Jacob advanced the notion that an oxide film permeated by Cl^- ions exhibits the ability to withstand high current densities. This phenomenon culminates in the formation of pits when the electric field exceeds a critical threshold at the interface between the film and the solution [67]. In a parallel line of inquiry, Sato delineated that thinner films tend to succumb to breakdown via the Zener mechanism, while thicker ones undergo avalanche breakdown when subjected to intense electric fields. Building upon this framework, Szklarska-Smialowska proposed that the adsorption of Cl^- ions triggers the injection of electrons into the passive film. Consequently, this process diminishes the optical breakdown potential to the level corresponding to the pitting potential [69].

Moreover, it has been postulated that the Zener mechanism, predominant in thinner regions, gives rise to elevated currents accompanied by significant heat generation. This thermal effect, in turn, contributes to the film's demise with an energetic discharge, often described as a "spark". Nevertheless, it is imperative to acknowledge that many existing theories, including some that are not expounded upon in this discussion, lack comprehensive experimental validation [70]. Thus, further empirical investigations are warranted to corroborate and refine these proposed mechanisms.

By combining experimental data and density functional theory (DFT) simulations, Maurice and Marcus [71] demonstrate how molybdenum, enriched in the nanometer-thick passive film, effectively enhances resistance to chloride-induced passivity breakdown. The presence of molybdenum in various oxidation states within the passive film influences ion transport, restricts chloride ion penetration, and encourages selective dissolution of iron, thereby promoting its replacement by more stable chromium and molybdenum species. Molybdenum, existing as Mo(IV/VI) and Cr(III) oxide species in the outer exchange and inner barrier layers of the passive film, respectively, helps curtail chloride ion infiltration into the oxide film. Research has demonstrated that the concentration of Mo and Cr oxides in these layers can confine chloride ion penetration solely to the outermost section of the oxide film. Additionally, molybdenum oxides on the surface inhibit the outward diffusion of chromium, thus impeding voiding mechanisms that could trigger passivity breakdown. Moreover, Mo oxides have been observed to suppress passive film dissolution, which serves as another avenue for passivity breakdown. These combined effects of molybdenum play a pivotal role in averting passivity breakdown in chloride solutions and enhancing the overall corrosion resistance of the materials

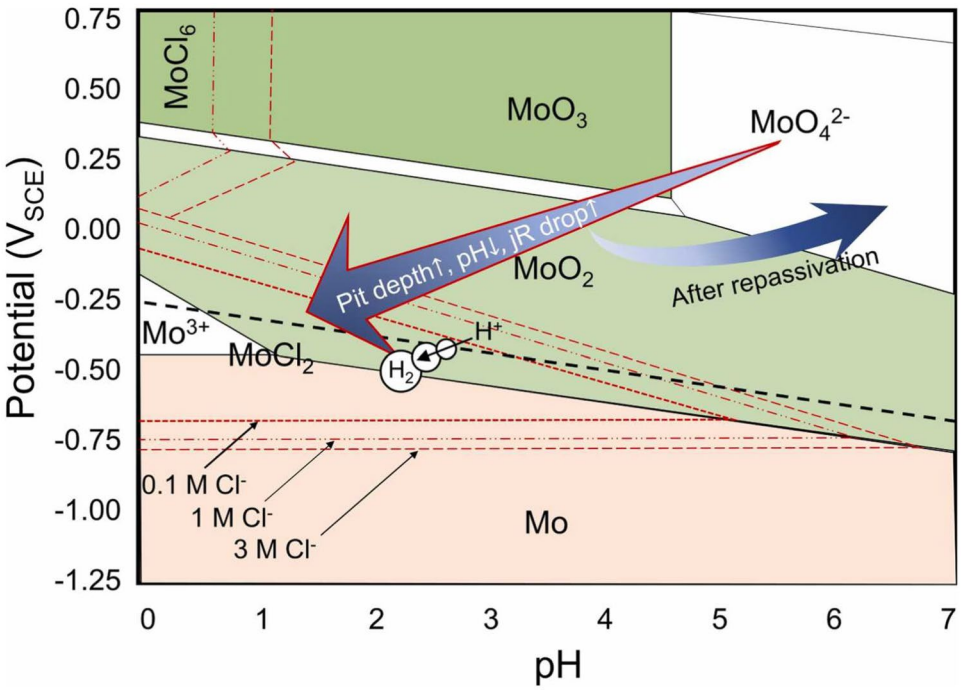

Fig. 22 The E-pH diagram for molybdenum in water with a solute concentration of 1 mM/L and varying chloride ion concentrations (25 °C, 1 atm) was forecasted using materialsproject.org. The arrows indicate changes in pit chemistry as the pit depth increases and after repassivation [72]

under investigation. In essence, molybdenum facilitates self-repair mechanisms within the passive film and boosts corrosion resistance by modulating ion transport, particularly that of chloride ions, within the oxide matrix. Atomic spectro-electrochemistry ASEC analysis carried out by Choudhary et al. [72] revealed a noticeable increase in the concentration of chromium (Cr) and molybdenum (Mo) during the initial or metastable phase of pit growth in SS316L. The elevated Mo concentration during initial pit growth might be associated with the development of Mo(IV/VI) oxides on the pit surface, triggered by a minor pH decline, as suggested by the E-pH diagram (Fig. 22). The precipitation of insoluble Mo oxides improves resistance against dissolution, thereby slowing down the pH decrease and promoting the formation of a protective layer consisting of Cr(III) oxide/oxyhydroxide on the surface. Subsequent to repassivation, there was an observed rise in the relative dissolution rate of Mo, potentially attributable to pH neutralization on the surface, leading to the dissolution of Mo(IV/VI) species. In addition, Choudhary et al. demonstrate the multifaceted nature of hydrogen's involvement in corrosion processes, highlighting the complex interplay between its effects on pit stability and repassivation. The study shows that increasing H^+ and Cl^- concentrations, coupled with a rising potential drop across the pit electrolyte, triggers the H_2 gas evolution reaction within the pit. However, a perforated cover obstructs the release of small H_2 gas bubbles, leading to their amalgamation into larger bubbles until rupture. This rupture enhances mixing of the pit solution, promoting repassivation. Pits in 0.1 M NaCl often grew with bulging covers, and repassivation frequently occurred through the expulsion of H_2 gas bubbles. While H_2 gas bubbles can stabilize pits, they can also rupture covers of smaller pits, increasing mixing and repassivation. Despite this, some pits continued to grow, indicating a complex interplay between H_2 gas evolution, pit growth, and cover rupture, warranting further investigation. This understanding could potentially inform the development of more effective corrosion prevention strategies and materials.

Conclusion

In this review paper, an overview of studies on the factors affecting MSS and SMSS passive film in the gas and oil fields are provided. From the literature study, it is evident that environmental parameters such as temperature, pH, sulfide, and chloride ion can lead to passivity breakdown. In the literature, they studied the surface morphology and elemental analysis using SEM and EDS, respectively, and the effect of environmental parameters was studied using the cyclic potentiodynamic studies. The following conclusions can be drawn from literature on SSC susceptibility in modified MSS alloys.

- This review explores pitting corrosion in stainless steel, highlighting the complex interplay of factors influencing corrosion susceptibility and resistance.
- The increased sulfide concentration at the fracture site of MSS shows that H_2S can make the specimens more susceptible to cracking under stress.
- For super martensitic stainless steels, electrochemistry is a very promising approach that meets the goal of reducing the time and cost associated with SSC performance evaluation.
- Modifying the chemical composition and heat treatment process of MSS can improve its mechanical properties and corrosion resistance.
- Cr content in the MSS may enhance its corrosion resistance and mechanical properties under high temperature and high pressure in a corrosive environment.
- It is observed that increasing the Cr and Mo content improves the formation and stabilization of the passive layer against pitting corrosion. However, above 3%, molybdenum precipitates with iron to form Fe_2Mo, reducing the alloy's corrosion resistance.
- The elucidation of crystallographic orientation's impact on pitting resistance highlights the importance of material texture optimization in mitigating corrosion risks.

Overall, there is a need for continued research efforts aimed at understanding corrosion mechanisms and developing effective protection strategies. By combining experimental data with theoretical insights, researchers can further advance our understanding of corrosion processes and enhance the durability of stainless steel and other materials in corrosive environments.

Acknowledgements The authors are very grateful to the Centre for Advanced Materials (CAM), Qatar University, for the inclusion.

Funding Open Access funding provided by the Qatar National Library. This study was made possible by NPRP grants NPRP12S0203-190038 from the Qatar National Research Fund (a member of Qatar Foundation) and Qatar University grant QUCD-IRCC-YSC-24–445. The findings made herein are solely the responsibility of the authors.

References

1. Sridhar N, Thodla R, Gui F et al (2018) Corrosion-resistant alloy testing and selection for oil and gas production. Corros Eng, Sci Technol 53:75–89. https://doi.org/10.1080/1478422x.2017.1384609
2. Askari M et al (2021) Downhole corrosion inhibitors for oil and gas production–a review. Appl Surf Sci Adv 6:100128. https://doi.org/10.1016/j.apsadv.2021.100128
3. Pessu F, Hua Y, Neville A, Barker R (2017) A study of the localized and uniform corrosion characteristics of X65 carbon steel in different H_2S-CO_2-containing environments. Corrosion 74:886–902. https://doi.org/10.5006/cj-1706-oa-2537.1
4. Zhang GA, Zeng Y, Guo XP et al (2012) Electrochemical corrosion behavior of carbon steel under dynamic high pressure H_2S/CO_2 environment. Corros Sci 65:37–47. https://doi.org/10.1016/j.corsci.2012.08.007
5. Fajardo S, Bastidas DM, Criado M, Bastidas JM (2014) Electrochemical study on the corrosion behaviour of a new low-nickel stainless steel in carbonated alkaline solution in the presence of chlorides. Electrochim Acta 129:160–170. https://doi.org/10.1016/j.electacta.2014.02.107
6. Machuca LL, Bailey SI, Gubner R (2012) Systematic study of the corrosion properties of selected high-resistance alloys in natural seawater. Corros Sci 64:8–16. https://doi.org/10.1016/j.corsci.2012.06.029
7. Palimi MJ, Peymannia M, Ramezanzadeh B (2015) An evaluation of the anticorrosion properties of the spinel nanopigment-filled epoxy composite coatings applied on the steel surface. Prog Org Coat 80:164–175. https://doi.org/10.1016/j.porgcoat.2014.12.003
8. Evans UR (1989) The reactive element effect on high temperature oxidation. Mater Sci Forum 43:243–268. https://doi.org/10.4028/www.scientific.net/MSF.43.243
9. Bramfitt BL (2005) Carbon and alloy steels. In Mechanical engineers' handbook: materials and mechanical design 1:1–38. https://doi.org/10.1002/0471777447.fmatter
10. Garrison Jr. WM (2001) Stainless steels: martensitic. Encyclopedia of materials: science and technology. Elsevier, pp 8804–8810. https://doi.org/10.1016/B0-08-043152-6/01582-5
11. Davydov A, Alekseeva E, Kolnyshenko V et al (2023) Corrosion resistance of 13Cr steels. Metals 13:1805. https://doi.org/10.3390/met13111805
12. Solheim KG, Solberg JK, Walmsley J et al (2013) The role of retained austenite in hydrogen embrittlement of supermartensitic stainless steel. Eng Fail Anal 34:140–149. https://doi.org/10.1016/j.engfailanal.2013.07.025
13. Soares RB, Lins VdFC (2017) Corrosion resistance of rolled and rerolled super martensitic steel in media containing chlorides and hydrogen sulfide. Matéria (Rio J) 22:1–11. https://doi.org/10.1590/s1517-707620170004.0232
14. Mesquita TJ, Chauveau E, Mantel M et al (2014) Corrosion and metallurgical investigation of two supermartensitic stainless steels for oil and gas environments. Corros Sci 81:152–161. https://doi.org/10.1016/j.corsci.2013.12.015
15. Taban E, Kaluc E, Ojo OO (2016) Properties, weldability and corrosion behavior of supermartensitic stainless steels for on-and offshore applications. Mater Test 58(6):501–518. https://doi.org/10.3139/120.110884
16. Anwar MS, Romijarso TB, Mabruri E (2018) Pitting resistance of the modified 13Cr martensitic stainless steel in chloride solution. Int J Electrochem Sci 13:1515–1526. https://doi.org/10.20964/2018.02.13
17. Monnot M, Nogueira RP, Roche V et al (2017) Sulfide stress corrosion study of a super martensitic stainless steel in H_2S sour environments: metallic sulfides formation and hydrogen embrittlement. Appl Surf Sci 394:132–141. https://doi.org/10.1016/j.apsusc.2016.10.072
18. Meena LK, Gorja SR, Bhardwaj A, Singh R (2024) Sour service domains of 13Cr martensitic stainless steels: a review of state-of-art knowledge vis-à-vis ANSI/NACE MR0175/ISO 15156. Trans Indian Inst Met. https://doi.org/10.1007/s12666-023-03253-0
19. Hudgins CM, McGlasson RL, Mehdlzadeh P, Rosborough WM (1966) Hydrogen sulfide cracking of carbon and alloy steels. Corrosion 22(8):238–251. https://doi.org/10.5006/0010-9312-22.8.238
20. Turnbull A, May AT (1990) The effect of temperature and H_2S content on the cracking resistance of a 13% chromium martensitic stainless steel in acidified NaCl. Corros Sci 30:657–665. https://doi.org/10.1016/0010-938x(90)90030-9
21. Tsai W-T, Chou S-L (2000) Environmentally assisted cracking behavior of duplex stainless steel in concentrated sodium chloride solution. Corros Sci 42:1741–1762. https://doi.org/10.1016/s0010-938x(00)00029-9
22. Kadhim MG, Ali MT (2021) A critical review on corrosion and its prevention in the oilfield equipment. Journal of Petroleum Research and Studies 7:162–189. https://doi.org/10.52716/jprs.v7i2.195
23. Shoesmith DW, Taylor P, Bailey MG, Owen DG (1980) The formation of ferrous monosulfide polymorphs during the corrosion of iron by aqueous hydrogen sulfide at 21°C. J Electrochem Soc 127:1007–1015. https://doi.org/10.1149/1.2129808
24. Liu ZY, Wang XZ, Liu RK et al (2014) Electrochemical and sulfide stress corrosion cracking behaviors of tubing steels in a H_2S/CO_2 annular environment. J of Materi Eng and Perform 23:1279–1287. https://doi.org/10.1007/s11665-013-0855-x
25. Ma H, Cheng X, Li G et al (2000) The influence of hydrogen sulfide on corrosion of iron under different conditions. Corros Sci 42:1669–1683. https://doi.org/10.1016/s0010-938x(00)00003-2
26. Marchebois H, Leyer J, Orlans-Joliet B, Deletombe P, Langrill C, De Montleber D (2006) SSC performance of a super 13% Cr martensitic stainless steel: Influence of PH2S, pH, and chloride content. Proceedings of the SPE International Oilfield Corrosion Symposium, pp 267–275 https://doi.org/10.2118/100646-MS
27. Wang Y, Li J, Cheng Y, He S (2015) Effect of pH and chloride on the micro-mechanism of pitting corrosion for high strength pipeline steel in aerated NaCl solutions. Appl Surf Sci 349:746–756. https://doi.org/10.1016/j.apsusc.2015.05.053
28. Mansour R, Elshafei AM (2016) Role of microorganisms in corrosion induction and prevention. Br Biotechnol J 14(3):1–11. https://doi.org/10.9734/BBJ/2016/27049
29. Lee W, Lewandowski Z, Nielsen PH, Hamilton WA (1995) Role of sulfate-reducing bacteria in corrosion of mild steel: a review. Biofouling 8:165–194. https://doi.org/10.1080/08927019509378271
30. Chen H, Kimyon O, Lamei Ramandi H et al (2021) Microbiologically influenced corrosion of cable bolts in underground coal mines: the effect of Acidithiobacillus ferrooxidans. Int J Min Sci Technol 31:357–363. https://doi.org/10.1016/j.ijmst.2021.01.006
31. AlAbbas FM, Williamson C, Bhola SM et al (2013) Influence of sulfate reducing bacterial biofilm on corrosion behavior of low-alloy, high-strength steel (API-5L X80). Int Biodeterior Biodegradation 78:34–42. https://doi.org/10.1016/j.ibiod.2012.10.014
32. Little BJ, Lee JS (2015) Microbiologically influenced corrosion. In Corrosion (pp. 387–398). https://doi.org/10.1002/9781119019213.ch27
33. Abdolahi A, Hamzah E, Ibrahim Z, Hashim S (2014) Application of environmentally-friendly coatings toward inhibiting the microbially influenced corrosion (MIC) of steel: a review. Polym Rev 54:702–745. https://doi.org/10.1080/15583724.2014.946188
34. Sagar SS, Kumar R, Kaistha SD (2016) Biofilm-an eternalchronicle of bacteria. Ind Jour Comparat Microbiol, Immunol and Infect Diseas 37:45. https://doi.org/10.5958/0974-0147.2016.00010.6
35. Kermani B, Cooling P, Martin JW, Nice PI (1998) The application limits of alloyed 13% Cr tubular steels for downhole

duties. CORROSION 98. OnePetro, p 98094. https://onepetro.org/NACECORR/proceedings-abstract/CORR98/All-CORR98/127672
36. Soares RB, Campos WRC, Gastelois PL, Macedo WAA, Dick LFP, Lins VFC (2020) Electrochemical properties of passive film formed on supermartensitic stainless steel in a chloride medium. Corrosion 76(9):884–890. https://doi.org/10.5006/3230
37. Sunaba T, Ito T, Miyata Y et al (2014) Influence of chloride ions on corrosion of modified martensitic stainless steels at high temperatures under a CO_2 environment. Corrosion 70:988–999. https://doi.org/10.5006/1141
38. Wang D, Zou DN, Tang CB et al (2011) Studies on corrosion behavior of S-165 and HP supermartensitic stainless steels in Cl^- environment. MSF 695:425–428. https://doi.org/10.4028/www.scientific.net/msf.695.425
39. Luo S, Fu A, Liu M et al (2021) Stress corrosion cracking behavior and mechanism of super 13Cr stainless steel in simulated O2/CO2 containing 3.5 wt% NaCl solution. Eng Fail Anal 130:105748. https://doi.org/10.1016/j.engfailanal.2021.105748
40. Oliveira J, Tchoundjeu S, Néel G et al (2018) Cost effective material selection for sour and sweet HPHT field. Proceedings of the SPE International Oilfield Corrosion Conference and Exhibition, p SPE-190914-MS. https://doi.org/10.2118/190914-MS
41. Mabruri E, Anwar MochS, Prifiharni S et al (2016) Tensile properties of the modified 13Cr martensitic stainless steels. Proceedings of the 3rd International Conference on Advanced Materials Science and Technology, p 020039. https://doi.org/10.1063/1.4945493
42. Rusnaldy ME, Nugroho LW (2019) Effect of heat treatment on the stress corrosion cracking (scc) susceptibiliy of the 13Cr martensitic stainless steel for steam turbine blade. IOP Conf Ser: Mater Sci Eng 547:012059. https://doi.org/10.1088/1757-899x/547/1/012059
43. Nishimura R, Katim I, Maeda Y (2001) Stress corrosion cracking of sensitized type 304 stainless steel in hydrochloric acid solution—predicting time-to-failure and effect of sensitizing temperature. Corrosion 57:853–862. https://doi.org/10.5006/1.3290312
44. Zhang Z, Zheng Y, Li J et al (2019) Stress corrosion crack evaluation of super 13Cr tubing in high-temperature and high-pressure gas wells. Eng Fail Anal 95:263–272. https://doi.org/10.1016/j.engfailanal.2018.09.030
45. Ma L, Liu H, Geng H et al (2020) Research and application of fracture failure control technology for 13Cr tubing in high temperature and high pressure gas wells. Presented at the International Petroleum Technology Conference, p IPTC-20136. https://doi.org/10.2523/iptc-20136-abstract
46. Zhao X, Huang W, Li G et al (2020) Effect of CO_2/H_2S and applied stress on corrosion behavior of 15Cr tubing in oil field environment. Metals 10:409. https://doi.org/10.3390/met10030409
47. Millet C, Gomes C, Decultieux F, Song S (2019) New supermartensitic alloy for high pressure high temperature applications. CORROSION 2019. https://onepetro.org/NACECORR/proceedings-abstract/CORR19/All-CORR19/NACE-2019-12782/127098?redirectedFrom=PDF
48. Tsay LW, Chi MY, Chen HR, Chen C (2006) Investigation of hydrogen sulfide stress corrosion cracking of PH 13–8 Mo stainless steel. Mater Sci Eng, A 416:155–160. https://doi.org/10.1016/j.msea.2005.10.021
49. JoséR G (1987) A stress corrosion cracking mechanism based on surface mobility. Corros Sci 27:1–33. https://doi.org/10.1016/0010-938x(87)90117-x
50. Hashizume S, Inohara Y (2000) Effects of pH and PH2S on SSC resistance of martensitic stainless steels. Paper presented at CORROSION 2000, p NACE-00130. https://onepetro.org/NACECORR/proceedings-abstract/CORR00/All-CORR00/111999
51. Sakamoto S et al (2002) Effect of environmental and material factors on SSC property of super 13Cr steel for OCTG. Sekiyu Gijutsu Kyokaishi 67(2):229–239. https://doi.org/10.3720/japt.67.229
52. Deffo Ayagou MD, Garcia DCS, Evin HN, Millet C, Néel G (2020) Fast screening of sulfide stress corrosion resistance of supermartensitic stainless steel through alternative test methods. Corrosion, p 225471981. https://api.semanticscholar.org/CorpusID:225471981
53. Rincon Flores P, Khoo CA, Gonuguntla M, Saithala JR, Hubaishi M, Behlani N, van Kuppevelt MA, Wilms ME, Grimes WD, Smit JP (2017) Application of the operating window of 13Cr4Ni1Mo 110 ksi well tubular in a mild sour gas environment. Proceedings of CORROSION, p 9242. https://onepetro.org/NACECORR/proceedings-abstract/CORR17/All-CORR17/NACE-2017-9242/125457
54. Kimura M, Tamari T, Yamazaki Y et al (2005) Development of new 15Cr stainless steel OCTG with superior corrosion resistance. Proceedings of the SPE Applied Technology Workshop on High Pressure/High Temperature Sour Well Design, p 98074. https://doi.org/10.2118/98074-ms
55. Monnot M, Roche V, Estevez R et al (2017) Molybdenum effect on the sulfide stress corrosion of a super martensitic stainless steel in sour environment highlighted by electrochemical impedance spectroscopy. Electrochim Acta 252:58–66. https://doi.org/10.1016/j.electacta.2017.08.165
56. Takabe H, Ueda M, Martin JW, Nice PI (2009) Application limits for 110ksi strength grade super 13Cr steel in CO_2 environments containing small amounts of H_2S. Proceedings of CORROSION, p 09083. https://onepetro.org/NACECORR/proceedings-abstract/CORR09/All-CORR09/NACE-09083/128559
57. Ishiguro Y, Suzuki T, Eguchi K, Nakahashi T, Sato H (2014) Martensite-based stainless steel OCTG of 15Cr-based and 17Cr-based material for sweet and mild sour condition. Eurocorr, p 7368. http://eurocorr.efcweb.org/2014/abstracts/10/7368.pdf
58. Isfahany AN, Saghafian H, Borhani G (2011) The effect of heat treatment on mechanical properties and corrosion behavior of AISI420 martensitic stainless steel. J Alloy Compd 509:3931–3936. https://doi.org/10.1016/j.jallcom.2010.12.174
59. Park J-Y, Park Y-S (2007) The effects of heat-treatment parameters on corrosion resistance and phase transformations of 14Cr–3Mo martensitic stainless steel. Mater Sci Eng, A 449–451:1131–1134. https://doi.org/10.1016/j.msea.2006.03.134
60. Kimura M, Miyata Y, Toyooka T, Kitahaba Y (2000) Effect of retained austenite on corrosion performance for modified 13% Cr steel pipe. Proceedings of CORROSION, p 00137. https://onepetro.org/NACECORR/proceedings-abstract/CORR00/All-CORR00/NACE00137/111993?redirectedFrom=PDF
61. Zou D, Han Y, Zhang W, Fang X (2010) Influence of tempering process on mechanical properties of 00Cr13Ni4Mo supermartensitic stainless steel. J Iron Steel Res Int 17:50–54. https://doi.org/10.1016/s1006-706x(10)60128-8
62. Horner DA, Lowden M, Nevitt P, Quirk G (2019) Hydrogen assisted cracking studies of a 12% chromium martensitic stainless steel—influence of hardness, stress and environment. Proceedings of the 18th International Conference on Environmental Degradation of Materials in Nuclear Power Systems–Water Reactors, pp 1051–1065. https://doi.org/10.1007/978-3-030-04639-2_66
63. Bösing I, Cramer L, Steinbacher M, Zoch HW, Thöming J, Baune M (2019) Influence of heat treatment on the microstructure and corrosion resistance of martensitic stainless steel. AIP Adv 9(6):065317. https://doi.org/10.1063/1.5094615

64. Zhang B, Wang J, Wu B et al (2018) Unmasking chloride attack on the passive film of metals. Nat Commun 9:2559. https://doi.org/10.1038/s41467-018-04942-x
65. Macdonald DD (1992) The point defect model for the passive state. J Electrochem Soc 139:3434–3449. https://doi.org/10.1149/1.2069096
66. Shahryari A, Szpunar JA, Omanovic S (2009) The influence of crystallographic orientation distribution on 316LVM stainless steel pitting behavior. Corros Sci 51:677–682. https://doi.org/10.1016/j.corsci.2008.12.019
67. Hoar TP, Jacob WR (1967) Breakdown of passivity of stainless steel by halide ions. Nature 216:1299–1301. https://doi.org/10.1038/2161299a0
68. Haruna T, Macdonald DD (1998) Breakdown of passive films on metals. Corros Eng 47:78–85. https://doi.org/10.3323/jcorr1991.47.78
69. Szklarska-Smialowska Z (2002) Mechanism of pit nucleation by electrical breakdown of the passive film. Corros Sci 44:1143–1149. https://doi.org/10.1016/s0010-938x(01)00113-5
70. Soltis J (2015) Passivity breakdown, pit initiation and propagation of pits in metallic materials – review. Corros Sci 90:5–22. https://doi.org/10.1016/j.corsci.2014.10.006
71. Maurice V, Marcus P (2024) Molybdenum effects on the stability of passive films unraveled at the nanometer and atomic scales. npj Mater Degrad 8:1–10. https://doi.org/10.1038/s41529-023-00418-6
72. Choudhary S, Kelly RG, Birbilis N (2024) On the origin of passive film breakdown and metastable pitting for stainless steel 316L. Corros Sci 230:111911. https://doi.org/10.1016/j.corsci.2024.111911